

# Two Degree-of-Freedom Control of Hard Disk Drive Servo Systems

Li Yi and Masayoshi Tomizuka

Mechanical Engineering Department

University of California,

Berkeley, CA 94720, U. S. A.

lyi@ME.Berkeley.EDU tomizuka@ME.Berkeley.EDU

## **Abstract**

This report proposes and investigates a two-degree-of freedom (2DOF) control structure for hard disk drive servo systems. This structure is applied to both track seeking and following control. It makes switches in mode switching control (MSC) found in conventional hard disk servo systems unnecessary. Two innovative features introduced in this reports are 1) a new method for generating reference signals for track seeking, and 2) two robust feedback control schemes for rejection of disturbances: one scheme uses a disturbance observer (DOB), and the other uses adaptive robust control (ARC).

A simulation study on a  $4.07kTPI$  (track per inch) NEC hard disk drive shows the effectiveness of 2DOF structure with ARC and DOB in both track seeking and tracking control. Comparisons are also made between ARC and DOB. Experimental results on a  $6.44kTPI$  Fujitsu hard disk drive setup confirm the advantage of the new reference generation method and the DOB based 2DOF structure. Another simulation study on a  $20kTPI$  hard disk drive validates the use of DOB for track following control of high density disk drives.

# Contents

<b>1</b>	<b>Introduction</b>	<b>3</b>
<b>2</b>	<b>Two-degree-of-freedom (2DOF) Servomechanism</b>	<b>6</b>
2.1	General Structure . . . . .	6
2.2	Reference Trajectory Generation . . . . .	9
2.3	Zero Phase Error Tracking Feedforward Controller . . . . .	12
2.4	Disturbance Observer . . . . .	14
2.5	Adaptive Robust Control Design . . . . .	17
<b>3</b>	<b>NEC Drive Simulation Study</b>	<b>20</b>
3.1	Plant Modeling . . . . .	20
3.2	Comparison between 2DOF and MSC . . . . .	21
3.3	Comparison between ARC and DOB . . . . .	23
<b>4</b>	<b>Fujitsu Drive Track Seeking Experimental Study</b>	<b>29</b>
4.1	Experimental Setup . . . . .	29
4.2	Implementation of the New Reference Generation Method . . . . .	30
4.3	Implementation of Disturbance Observer . . . . .	31
<b>5</b>	<b>High Capacity Drive Track Following Simulation Study</b>	<b>35</b>
5.1	Plant Modeling . . . . .	35

5.2	Disturbance Observer Design . . . . .	36
5.3	Analysis of simulation results . . . . .	39
<b>6</b>	<b>Conclusions</b>	<b>49</b>
<b>A</b>	<b>MATLAB function tools</b>	<b>53</b>
A.1	Zero Phase Inversion (f_zp_inv.m) . . . . .	53
A.2	Decouple Signals into Repetitive and Non-repetitive Portions (fsig2rro.m) . .	53
A.3	Q filter for Disturbance Observer (f_qfilter.m) . . . . .	53
A.4	ZOH model with Input Delay (f_zoh_td.m) . . . . .	53

# Chapter 1

## Introduction

Hard disk servo systems play a vital role for meeting the demand of increasingly high density and high performance hard disk drives. Components in a typical hard disk drive are shown in Figure 1.1. The servo system must achieve precise positioning of the read/write head on a desired track for track following, and fast transition from one track to another target track for track seeking. The transition time, or seek time, should be minimized for faster data transfer rates. Because of the different objectives during track seeking and following, the control algorithm for seeking is often different from that for following. The overall servo system then involves switches between algorithms, which is referred to as mode switching control (MSC). In MSC, nonlinear controllers such as proximate time optimal servo (PTOS)[1], are popular choices for track seeking. For track following, adaptive control[2][3], repetitive control[4], and many other approaches have been studied. Switching from seeking mode to following mode is often problematic and may cause undesired transients at the beginning of the settling or following mode. Such transients make the effective seek time longer.

This report focuses on the design of a unifying controller structure, a two-degree-of-freedom (2DOF) servomechanism, for both track seeking and following control. Disturbance observer (DOB)[5][6] and Adaptive Robust Control (ARC) are used in the 2DOF servomechanism as a part of the feedback controller. Zero Phase Error Tracking (ZPET) [7][5] technique is used to design the feedforward controller.

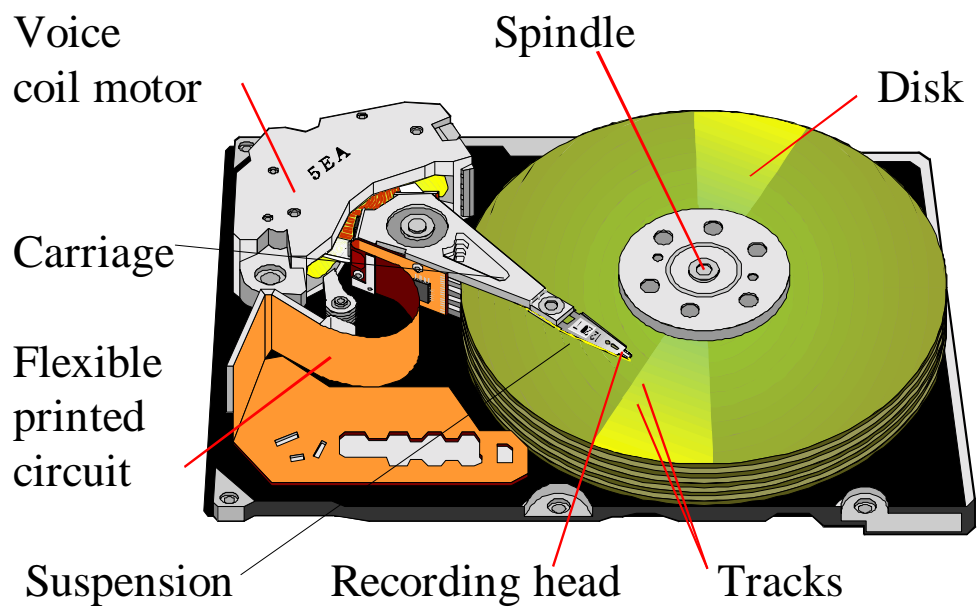


Figure 1.1: Hard Disk Drive Components.

Embedded servo is now popular for hard disk drives with high track densities. In embedded servo systems, position signals are embedded in circular data tracks at equally spaced angles; equally divided areas of a circular disk are called sectors. The disk rotates at a fixed spindle speed. As a result, embedded servo systems are discrete in nature, and the product of the spindle speed and the number of sectors determines the sampling rate for the digital servo control. The number of sectors should be minimized to achieve the maximum data storage area. Under this constraint, ideas such as multi-rate control and feedback control based on other sensors[8] are useful for performance enhancement. Feedforward control is an important element of the 2DOF servomechanism. The feedforward controller is tuned according to the closed-loop dynamics, which is based on the knowledge of the nominal plant model. External disturbances and parameter variations are not considered in its design. DOB has been proven work well to handle low frequency external disturbances and parameter variations in many industry applications such as machine tools. The goal of DOB or ARC, in the feedback loop, is to let the plant dynamics minimally affected by model uncertainties and external disturbances such as uncompensated friction or external shocks. Compared with DOB, ARC can handle larger parameter variations and offers more flexibility because of the presence of extra nonlinear robust control terms and parameter adaptations to improve the transient response and tracking performance. Anti-integration windup mechanisms are built into ARC, and control saturation problems are alleviated.

The remainder of this report is organized as follows. 2DOF general structure, including a new reference generation method, ZPET, DOB and ARC, are discussed in Chapter 2. A simulation study on a  $4.07kTPI$  NEC drive in Chapter 3 shows the effectiveness of 2DOF structure with DOB and ARC. Comparisons of DOB and ARC are also made. In Chapter 4, experimental results on a  $6.44kTPI$  Fujitsu hard disk setup confirm the advantage of 2DOF with DOB for track seeking control. In Chapter 5, a simulation study on a high capacity  $20kTPI$  hard disk drive shows the effectiveness of the DOB for track following control. Conclusions are given in Chapter 6. Useful MATLAB scripts are provided in Appendix A.

# Chapter 2

## Two-degree-of-freedom (2DOF) Servomechanism

### 2.1 General Structure

The goal of a unifying controller working for both track seeking and following without mode changes is to assure smooth motion of the read/write head avoiding exciting high frequency dynamics, and minimizing residual vibration.

In the track following mode the head must remain precisely on the track center, while the track seeking mode the head must make fast and smooth transition from one track center to another. It is a common practice to design two different sets of controllers for these two modes and optimize them based on the distinctive requirements. This approach results in Mode Switching Control (MSC), which is conventional in the current disk servo systems. The MSC scheme is illustrated in Figure 2.1.

In conventional MSC, a seek velocity profile is specified by a function or a lookup table of the remaining distance to the target track. For protection of the read/write head, its velocity should remain under a limit, called the coast velocity. When the head is commanded to start a long seek, the maximum voltage is applied to the VCM carriage for the maximum acceleration. The head is accelerated quickly at almost a constant rate. When the velocity



reaches the coast velocity even before it reaches the velocity reference profile, the voltage drops to zero and the head moves at a constant velocity around the coast level. The head velocity will eventually hit the reference velocity profile, either before or after it reaches the coast line. At that stage, the servo ends the open loop push and/or hold action and switches to closed-loop velocity control. The head velocity control follows the reference velocity profile until the head comes close to the target track within a predefined distance from the track center. Then the servo switches to the track following controller, which is usually a PID or state feedback controller plus some notch filters.

In MSC, the velocity profile and switching conditions are crucial for smooth transients of the head motion. They are usually designed based on trial and error and their effectiveness relies on the engineer's experience. Efforts have been made for systematic design methods, such as Initial Value Compensation (IVC) at the mode switching instance[9].

This report proposes and investigates a two-degree-of-freedom (2DOF) servomechanism structure which may be applied to both track seeking and track following. It is configured as shown in Figure 2.2. Note that it includes three major components: 1) feedback controller; 2) feedforward controller, and 3) reference generator. The advantages of 2DOF over MSC are: 1) 2DOF control avoids mode changes, and therefore avoids abrupt changes of the control input which may excite high frequency resonance modes of the suspension, which creates acoustics problems; 2) systematically designed reference profile and feedforward control can be applied; and 3) robust feedback controller is integrated in the 2DOF control structure.

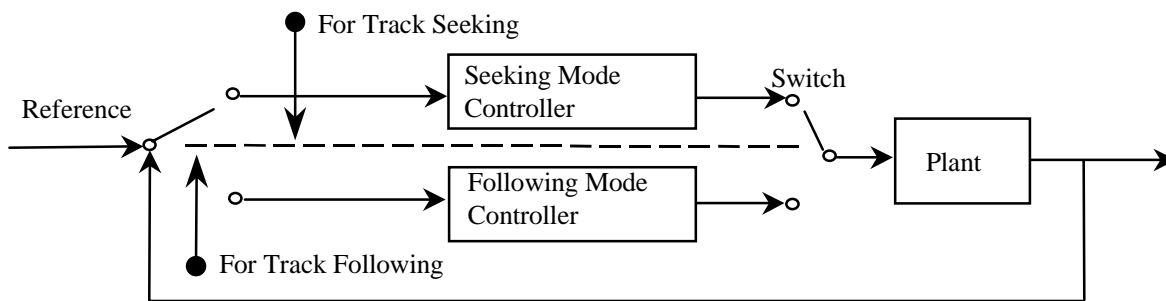


Figure 2.1: Mode Switching Control (MSC) structure.

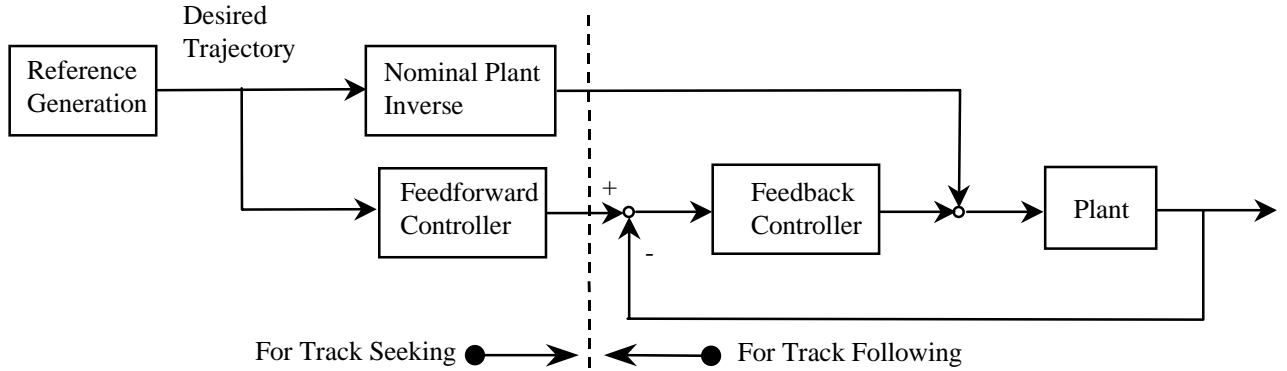


Figure 2.2: Two-degree-of-freedom servomechanism structure.

Figures 2.3 and 2.4 illustrate two implementation forms of the proposed 2DOF structure: one is with Disturbance Observer (DOB) and the other with Adaptive Robust Control (ARC). The plant is represented by  $G_p(z^{-1})$  in Fig. 2.3 and by  $\frac{1}{Js^2+Bs}$  in Fig. 2.4. The difference is due to the design of DOB and ARC, which will be discussed later in Chapter 3. As illustrated in Fig. 2.3 and Fig. 2.4, 2DOF servomechanism consists of three major components: the first one is the robust velocity feedback controller, which uses either DOB or ARC, plus the position loop feedback controller  $G_c$ ; the second is the feedforward controller, plus a bias feedforward compensator; and the third one is a reference generator. The reference generator supplies the desired output for track seeking. The bias compensator is a model based feedforward compensator for pivot friction and Flexible Printed Circuit (FPC, see Fig. 1.1) tension. This compensator does not require a very accurate model since DOB or ARC handles modeling errors.

The combined use of the feedforward controller and DOB/ARC is motivated by their distinctive but mutually benefiting advantages: the feedforward controller initiates control action based on model prediction, while DOB/ARC ensures that the model based feedforward controller design remains effective. DOB/ARC makes the plant dynamics remain unperturbed in the presence of model uncertainties and external vibrations. This also makes it easier to design the position loop controller  $G_c$ , which sees the nominal dynamics to control.

It can be seen from the Fig. 2.3 and Fig. 2.4 that the 2DOF servomechanism is basically a unified position tracking system. Performance requirements and velocity constraints of seeking and settling modes will be all reflected in the position signal performance requirements and constraints. In such a situation, reference signal generation plays a crucial role.

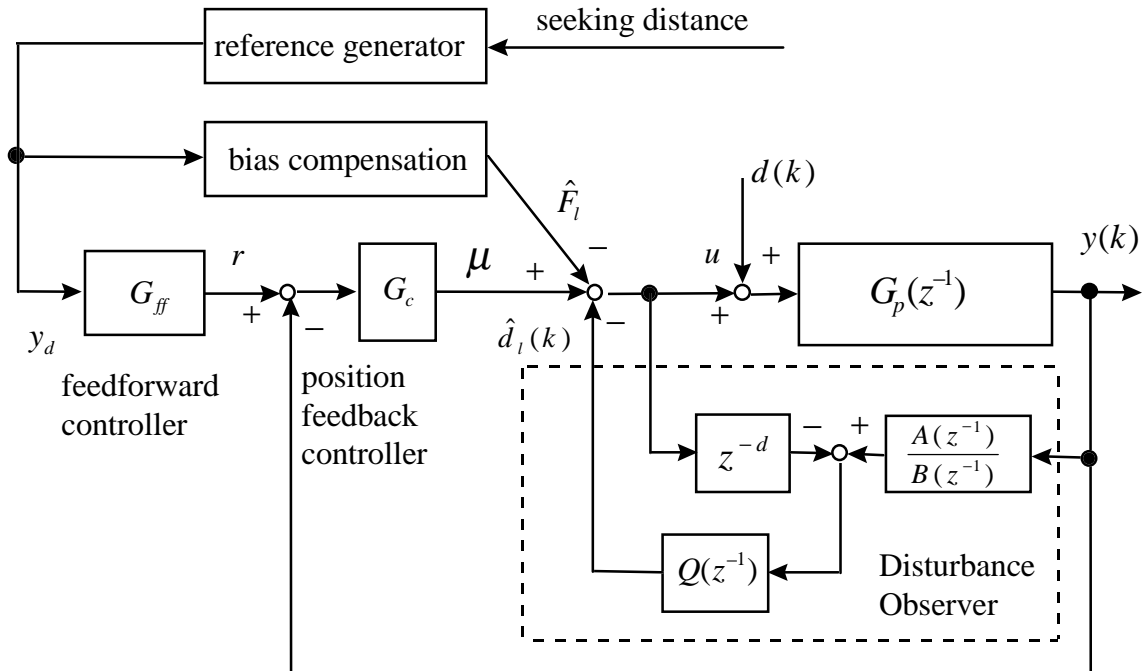


Figure 2.3: 2DOF structure with DOB

## 2.2 Reference Trajectory Generation

During the seeking mode of MSC, the servo controller drives the read/write head to follow a desired velocity profile calculated based on a rigid body plant model. For example, by defining the velocity profile as  $v(p) = -\text{sgn}(p)\sqrt{2a|p|} - r_t$  if  $|p| > \frac{2r_t^2}{a}$  or  $v(p) = -\frac{a}{2r_t} \cdot p$  if  $|p| \leq \frac{2r_t^2}{a}$ , a proximate time optimal servomechanism (PTOS) can be obtained[1].  $p$ ,  $a$ , and  $r_t$



are the remaining distance to the target track, the maximum acceleration, and the velocity offset, respectively. In the PTOS approach, the back e.m.f., which physically behaves like friction and can help to shorten the deceleration time, and the actuator bandwidth are not taken into consideration. As a result, the velocity profile in PTOS method can only be approximately followed.

Figure 2.5 shows a reference generator for the 2DOF control in this report. This reference generator provides the desired seek position as well as desired velocity and current profiles. The *Back e.m.f.* (electro-motive force) of the voice coil motor (VCM) is also taken into consideration and utilized to shorten the deceleration time. Reference trajectory for 2DOF servomechanism should 1) be aggressive to make the seek time short and at the same time achievable by the actuator with saturation and limited bandwidth; 2) make use of the back e.m.f. effects, which can help decrease the deceleration time for seeking; 3) be smooth enough not to excite high frequency resonant modes, and 4) not be too complicated because of hardware constraints such as computing power and memory of the on-board DSP.

The proposed reference model is used in two stages: off-line simulations and on-line reference generation. The reference model in Fig. 2.5 is motivated by the worst case operational condition in terms of power amplifier saturation. The bandwidth of the admittance transfer function  $\frac{1}{Ls+R}$  corresponds to the case where VCM is operating during amplifier saturation. Otherwise the reference model is a simplified nominal plant model.  $J$  is the inertia of the carriage arm.  $K$  and  $B$  are linearized spring and viscous friction terms representing the nonlinear pivot friction torque, which depends on both the position and the velocity [8].

As pointed out in [10], there is no closed form expression for a voltage-constrained deceleration velocity profile in terms of the remaining head travel distance to destination. However, the profile and the reference trajectory can be numerically determined off-line by simulations, and a look-up table with data extracted from the simulations can be made for on-line reference generation. The simulation procedures are: 1) impose a maximum positive voltage for acceleration, 2) if the velocity reaches the safety limit  $V_{max}$ , change the voltage to maintain the speed ( $U = K_{eb} * v$ ), 3) when the sample number reaches an appropriate number  $K_{sw}$  (switching sample), apply the minimum voltage for deceleration until the velocity

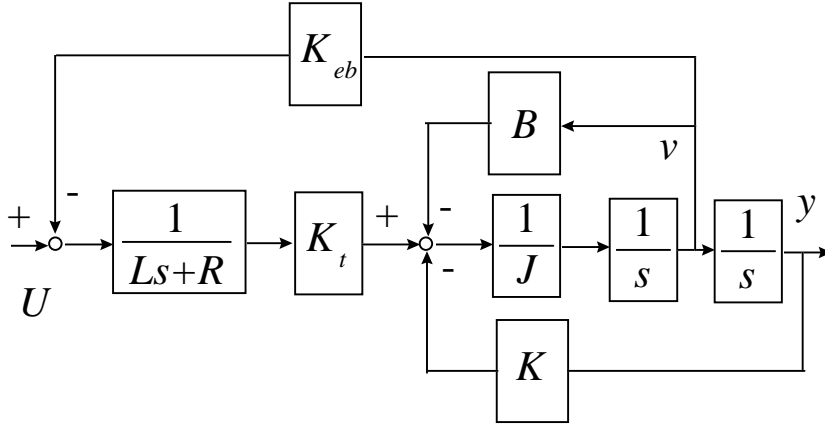


Figure 2.5: Reference generator considering back *e.m.f.* effects

reaches zero; 4) stop the simulation, record the switch sample, the final reached distance, the final time, etc. The maximum velocity limit here is for protection of the read/write head from crash damage in the event of a power failure. From repeated simulations with different  $K_{sw}$ , a look-up table can be created. This table is used for the on-line reference generator, in which the same model is used. Given the seeking distance command, the switch sample  $K_{sw}$  can be looked up from the table created by off-line simulations. The control input  $U$  changes according to the table values and the resulted output can be used as desired reference signal.

With the use of this new reference generation method, track seeking time can be reduced compared with the PTOS. Improvement is mostly achieved in the deceleration period due to the use of *back e.m.f.* Simulation comparisons are made in Section 3.2 and shown in Figure 3.2. Experimental comparisons are made in Section 4.2 and shown in Figure 4.1.

## 2.3 Zero Phase Error Tracking Feedforward Controller

The feedforward controller (see Figure 2.3 or 2.4) shapes the desired output to compensate for the dynamic lag of the closed loop system. For low sampling rate systems such as sector servos, feedforward control plays an important role in reference following. Let a closed loop

system be expressed as

$$G_{clp} = \frac{z^{-d}B(z^{-1})}{A(z^{-1})} \quad (2.1)$$

where

$$\begin{aligned} A(z^{-1}) &= 1 + a_1z^{-1} + a_2z^{-2} + \dots + a_nz^{-n} \\ B(z^{-1}) &= b_0 + b_1z^{-1} + b_2z^{-2} + \dots + b_mz^{-m} \end{aligned}$$

and  $z^{-1} = e^{-sT}$ .  $z^{-1}$  may be interpreted as a one-step delay operator. Then referring to Figure 2.3, for disturbance  $\widehat{F}_l$  and  $d(k) = 0$ ,

$$y(k) = -a_1y(k-1) - \dots - a_nz^{-N} + b_0r(k-d) + \dots b_mr(k-d-m)$$

If it is desired that the actual output  $y(k)$  follows the desired output  $y_d(k)$ , the ideal feedforward controller is the inverse of  $G_{clp}(z^{-1})$ , i.e.

$$G_{ff}(z^{-1}) = \frac{z^d A(z^{-1})}{B(z^{-1})}$$

Assuming that  $y_d(k)$  is known  $d$  steps in advance of  $y(k)$ , the feedforward controller can be implemented as

$$\begin{aligned} r(k) &= -b_0r(k) - \dots - b_mr(k-m) + y(k+d) + a_1y(k+d-1) + \dots + a_ny(k+d-n) \\ &= -b_0r(k) - \dots - b_mr(k-m) + y_d(k) + a_1y_d(k-1) + \dots + a_ny_d(k-n) \end{aligned}$$

The transfer function from  $y_d$  to  $y$  is then

$$G_{ff}(z^{-1})G_{clp} = \frac{z^d A(z^{-1})}{B(z^{-1})} \cdot \frac{z^{-d}B(z^{-1})}{A(z^{-1})} = 1$$

which implies  $y(k) = y_d(k)$  under ideal conditions.

Unfortunately, the ideal feedforward controller above can not be implemented when  $B(z^{-1})$  possesses any zero outside the unit circle (unstable zeros). The zero phase error tracking (*ZPET*) controller is an easy to implement feedforward controller in this situation. To introduce the idea of *ZPET*, the closed loop transfer function is written as

$$G_{clp}(z^{-1}) = \frac{z^{-d}B^+(z^{-1})B^-(z^{-1})}{A(z^{-1})}$$

where  $B^-(z^{-1})$  contains all zeros outside of the unit circle and  $B^+(z^{-1})$  contains all zeros inside of it. The ZPET controller is [7]

$$G_{ZPET}(z^{-1}) = \frac{z^d A(z^{-1}) B^-(z)}{[B^-(1)]^2 B^+(z^{-1})}$$

where  $B^-(z)$  is obtained by replacing every  $z^{-1}$  in  $B^-(z^{-1})$  by  $z$ .

The resulting transfer function from  $y_d$  to  $y$  (see Figure 2.3 or 2.4)

$$G_{clp}(z^{-1}) G_{ZPET}(z^{-1}) = \frac{B^-(z^{-1}) B^-(z)}{[B^-(1)]^2}$$

has the zero phase characteristics: i.e. it does not introduce any phase shift for sinusoidal inputs. Note that the ZPET controller cancels the closed loop poles, stable zeros, and the phase shift due to unstable zeros. MATLAB function to implement zero phase inversion is given in Appendix A.

## 2.4 Disturbance Observer

The disturbance observer (DOB) estimates the disturbance by subtracting the known input from the estimated total input to the plant. The total input is obtained by processing the plant output by the inverse of the nominal plant model. The disturbance estimate is used to cancel the disturbance. The continuous-time domain DOB structure is shown in Figure 2.6. An equivalent block diagram is shown in Figure 2.7. Signal  $c$ ,  $u$ ,  $d$ ,  $n$  and  $y$  are the DOB output, disturbance, sensor/position noise, and position output, respectively.  $G_p(s)$  is the plant to be controlled, the nominal model of which is  $G_n(s)$ . This nominal plant model may be a low order approximation of the actual plant.  $Q(s)$  is a low pass filter, and it is required to make DOB physically implementable. Note that  $G_n^{-1}(s)$  in Fig. 2.6 is normally an unrealizable transfer function (i.e., the numerator order exceeds the denominator order), but that  $Q(s)G_n^{-1}(s)$  can be made realizable by selecting the relative degree of  $Q(s)$  appropriately. Actually,  $Q(s)$  is designed to compromise disturbance rejection, noise attenuation and stability robustness. A popular Q filter is

$$Q(s) = \frac{(3\tau s + 1)}{(\tau s)^3 + 3(\tau s)^2 + 3\tau s + 1}$$



where  $\tau$  is the time constant, which is the major tuning parameter of DOB. From Figure 2.7, the following transfer functions can be derived:

$$\begin{aligned} G_{cy}(s) &= \frac{G_p(s)G_n(s)}{G_n(s) + Q(s)G_p(s) - Q(s)G_n(s)} \\ G_{dy}(s) &= \frac{G_p(s)G_n(s)(1 - Q(s))}{G_n(s) + Q(s)G_p(s) - Q(s)G_n(s)} \\ G_{ny}(s) &= \frac{G_p(s)Q(s)}{G_n(s) + Q(s)G_p(s) - Q(s)G_n(s)} \end{aligned}$$

where  $G_{\cdot y}(s)$  denotes the transfer function from  $\cdot$  to  $y$ .

It can be found that as  $Q(s)$  approaches 1 at low frequencies,  $G_{cy}(s)$  approaches  $G_p(s)$  and  $G_{dy}(s)$  approaches 0. As  $Q(s)$  approaches 0 at high frequencies,  $G_{ny}(s)$  approaches 0. Figure 2.7 shows that DOB closes a high gain inner loop around the plant at frequencies where  $Q(s) \approx 1$ . Assuming  $G_p(s) = G_n(s)$ , from Figure 2.7, it is easy to derive that the sensitivity function for the DOB loop is  $1 - Q(s)$ , and the complimentary sensitivity function is simply  $Q(s)$ . Open loop dynamics of the DOB loop is  $Q(s)/(1 - Q(s))$ . To ensure that the DOB loop is stable, the infinity norm of  $Q(s)\delta(s)$  should be less than 1, where  $\delta(s)$  is the multiplicative perturbation of the plant. i.e.

$$G_p(n) = G_n(s)(1 + \delta(s))$$

As mentioned in Introduction, sector servo systems are discrete in nature. As a result, the discrete-time domain disturbance observer (DOB) is used in this study (see Figure 2.3). A zero-order-hold equivalent discrete model of the plant is used and denoted as

$$G_p(z^{-1}) = \frac{z^{-d}B(z^{-1})}{A(z^{-1})} (1 + \Delta(z^{-1}))$$

where the uncertain dynamics of the plant is modelled with a multiplicative uncertainty,  $\Delta(z^{-1})$ , which is assumed to be a stable discrete transfer function. DOB cancels the external disturbance  $d$  by its estimate. Analogous to the continuous time case, the estimate is obtained by comparing the control signal  $u$  with the estimated input synthesized by the nominal inverse of the plant output. The difference between these two signals,  $\hat{d}_i$ , includes the

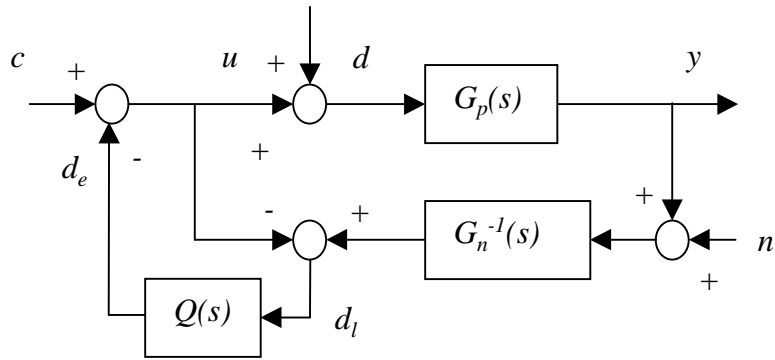


Figure 2.6: Continuous Time Disturbance Observer.

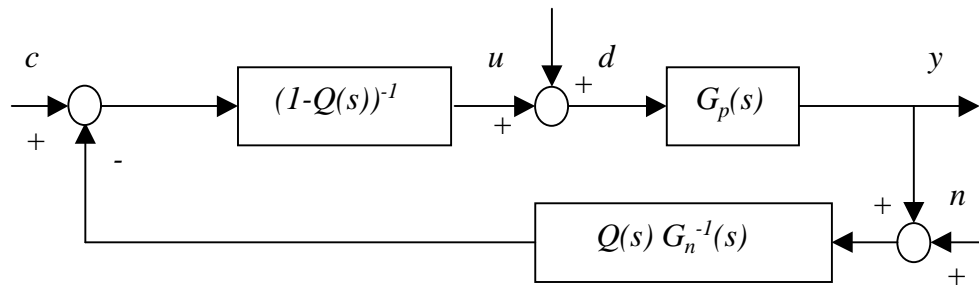


Figure 2.7: Alternative Representation of Continuous Time Disturbance Observer.

estimate of  $d$  as well as that of an equivalent disturbance to model uncertainties. At low frequencies, DOB forces the inner loop to approximate a nominal open loop plant from control input voltage  $u$  to position signal  $y$ .  $Q(z^{-1})$  is selected to have a value close to 1 at low frequencies, and have a value close to zero at higher frequencies to eliminate the effects of the measurement noise. The bandwidth of the low pass filter  $Q(z^{-1})$  determines the overall performance of the DOB.

If  $G_p(z^{-1})$  possesses unstable zeros, the zero phase inversion idea introduced in Section 2.3 can be used. MATLAB function to implement the zero phase inversion is given in Appendix A.

## 2.5 Adaptive Robust Control Design

The adaptive robust controller (ARC) is configured as illustrated in Figure 2.4. As in the DOB design, the objective of ARC is to synthesize a control input  $u$  such that the resulting system from  $\mu$  to  $y$  behaves like its nominal model, even under the presence of the external disturbance  $d$ . Considering the simplified model of the hard disk system

$$J \ddot{y} + B \dot{y} = u + d$$

we want

$$J_n \ddot{y} + B_n \dot{y} = \mu \tag{2.2}$$

where  $J_n$  and  $B_n$  are the nominal values of  $J$  and  $B$ , respectively. To gain insight about the proposed ARC and its advantages, we assume that the variations of  $J$  and  $B$  can be neglected in the design, i.e.,  $J = J_n$  and  $B = B_n$ . Dealing with the bounded disturbance  $d$  is emphasized in this design. Define a switching-function-like quantity  $p$  as

$$p = \dot{y} + \lambda y - \frac{1}{J_n} \int_0^t \mu(\tau) d\tau \tag{2.3}$$

where  $\lambda = \frac{B_n}{J_n}$ . Then

$$J_n \dot{p} = u + d - \mu \tag{2.4}$$

If  $\dot{p} = 0$ , then we have the desired relationship in (2.2). If all signals involved are uniformly continuous, then  $p \rightarrow 0$  means  $\dot{p} \rightarrow 0$ . Therefore,  $u$  could be synthesized by feedback control such that  $p$  is as small as possible. Let the control law be

$$u = u_s + u_f, \quad u_s = -Kp, \quad u_f = \mu - \widehat{F}_l - \widehat{d}_l \quad (2.5)$$

where  $K > 0$ ,  $\widehat{F}_l$  is any fixed bias compensation, and  $\widehat{d}_l$  is the estimate of the lumped uncompensated disturbance  $d_l = d - \widehat{F}_l$ .  $d_l$  is bounded and can be assumed that

$$d_l \in [d_m, d_M]$$

where  $d_m$  and  $d_M$  are known constants. From (2.5) and (2.4), the  $p$  dynamics is

$$J_n \dot{p} + Kp = -\widetilde{d}_l \quad (2.6)$$

where  $\widetilde{d}_l = \widehat{d}_l - d_l$  is the estimation error.

Equation (2.6) is a stable first-order system with respect to  $p$  with a bounded uncompensated disturbance input  $\widetilde{d}_l$  if fixed  $\widehat{d}_l$  is used. From

$$|p(\infty)| \leq \widetilde{d}_l(\infty)/K$$

$p$  can be made as small as possible by increasing feedback gain  $K$ . The modeling uncertainties are addressed by the robust feedback control. However in practice,  $K$  can not be arbitrarily large. Once  $K$  is fixed, the final tracking error  $p$ , is proportional to the size of the modeling uncertainty  $\widetilde{d}_l$ . In order to further improve performance, an adaptive algorithm can be added to make a better estimate of the lumped disturbance  $\widehat{d}_l$ . We can update  $\widehat{d}_l$  on-line by the following adaptation law

$$\dot{\widehat{d}}_l = \begin{cases} 0 & \text{if } (\widehat{d}_l = d_M \text{ and } p > 0) \text{ or } (\widehat{d}_l = d_m \text{ and } p < 0) \\ \Gamma p & \text{otherwise} \end{cases} \quad (2.7)$$

where  $\Gamma > 0$  is the adaptation rate. It can be proved in the same way as in [11] that if the disturbance is constant, the modeling uncertainty  $\widetilde{d}_l$  converges to zero and zero final tracking

error can be obtained for any feedback gain  $K$ . If  $d_m < \widehat{d}_i(t) < d_M$  for all  $t$ , then the error dynamics is

$$J_n \dot{p} + Kp + \Gamma \int_0^t p dt = d_i \quad (2.8)$$

Thus, the adaptation law can be interpreted as adding an integrator of  $p$ . Further remarks on *ARC* can be found in [11].

# Chapter 3

## NEC Drive Simulation Study

### 3.1 Plant Modeling

Simulations have been performed on a NEC hard disk drive model. The disk has a track-to-track pitch  $6.245\mu m$ , and the corresponding track density is  $4.07kTPI$ . It has a spindle speed of  $7200\ rpm$ , and a sampling time  $80\mu s$ . A simplified plant model is shown in Figure 3.1, where  $I_b$  is the moment of inertia of the mechanical carriage arm,  $D_b$  is the viscous friction coefficient, and  $K_b$  simulates a linear model of the pivot friction and the flexible printed circuit (FPC) tension. The VCM block is a second order linear system simulating the voice coil motor.  $K_{eb}$  is the back e.m.f. constant.  $K_t$  is the torque constant. Other parameters,  $G_{in}$ ,  $K_{in}$ ,  $G_{op}$ ,  $P_1$ ,  $AMP$  and  $K_{fb}$ , are constants related to the power amplifier. Resonant modes at about  $4kHz$  and higher frequencies are not shown in this model. The nonlinear pivot friction model found in [8] is used. This model may represent nonlinear rolling friction which has an upper and lower bound and a hysteresis characteristic within a small displacement range after the read/write head changes moving directions. For controller design purpose, the power amplifier and VCM can be assumed to be a constant gain, and the nonlinear pivot friction can be modeled as a linear spring. The model can therefore be simplified to  $\frac{1}{Js^2+Bs+K}$ , where  $J$ ,  $B$ ,  $K$  are the equivalent inertia, the equivalent friction coefficient, and the equivalent spring constant from  $u$  to  $y$ , respectively. If we ignore the



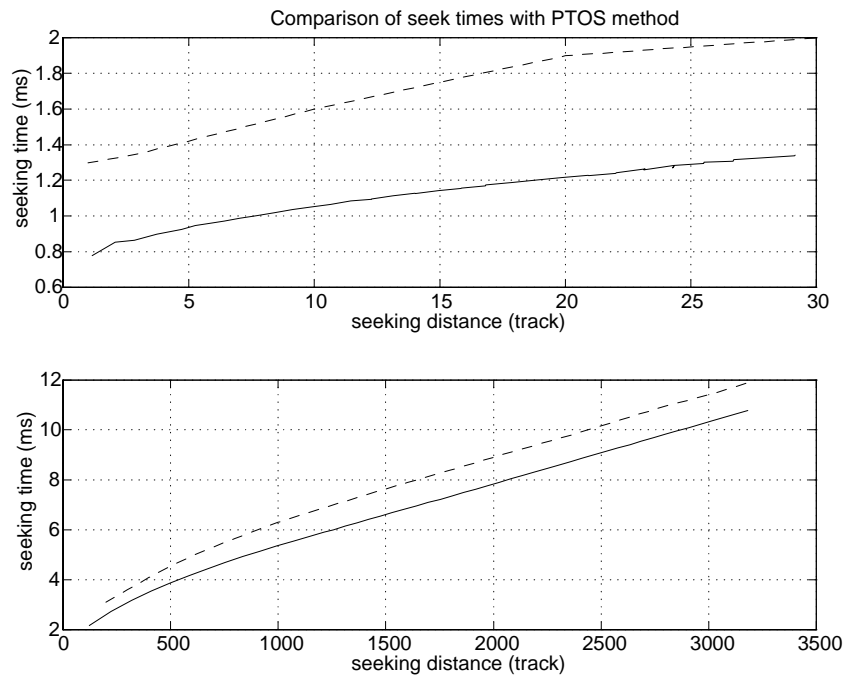


Figure 3.2: Simulation comparison of seek time of 2DOF with that of MSC, using NEC hard disk model



### 3.3 Comparison between ARC and DOB

For comparison of simulation results for different controllers, the following performance index are used. They are the average tracking performance index

$$L_2[e] = \sqrt{\frac{\sum_N e^2(k)}{N}} \quad (3.1)$$

with unit of track, the maximum tracking error  $e_M$  (track), the normalized control variations

$$L_2[\Delta u] = \sqrt{\frac{1}{N} \sum_N [u(k) - u(k-1)]^2} \quad (3.2)$$

and the control input chattering index

$$c_u = L_2[\Delta u] / L_2[u] \quad (3.3)$$

During simulations, an uncompensated bias  $0.1V$  (equivalent to torque  $0.0078Nm$ ) is present from  $0ms$ , and an external shock  $0.2V$  (equivalent to torque  $0.0156Nm$ ) enters the control input channel after  $5ms$ . A white noise with a variance  $0.1 mV$  also appears in the control input channel.

The feedback controller  $G_c$  is designed such that the resulting nominal closed-loop transfer function is critically damped with a corner frequency at  $800Hz$ . ZPET is designed by treating a zero near the unit circle as an uncancellable zero. In the *DOB* design, the  $Q$  filter is chosen as

$$Q(s) = (3\tau s + 1) / ((\tau s)^3 + 3(\tau s)^2 + 3\tau s + 1) \quad (3.4)$$

where  $\tau$  is set to make  $Q(s)$  have a bandwidth at about  $1200Hz$ , i.e.,  $\tau = 0.15 ms$ .  $Q(s)$  is then transformed into the discrete-time domain using the bilinear transformation. For *ARC* design,  $K$  and  $\Gamma$  are chosen to make the dynamics in (2.8) have a bandwidth at about  $800Hz$ . *ARC* controller is designed in the continuous time domain and transformed into discrete-time domain using the forward euler approximation. Considering the physical

meaning of the bounds of the estimated disturbance,  $d_M$  is set to 0.5 *Volts* and  $d_m$  is set to  $-0.5$  *Volts*.

Simulations are performed for each of the following 6 sets. Each set has a track seeking phase and a track following phase. Set 1, 1 track seek with nominal plant; Set 2, 1 track seek with 20% actuator gain variation. Set 3, 8 tracks seek with nominal plant; Set 4, 8 tracks seek with 20% actuator gain variation; Set 5, 1000 tracks seek with nominal plant, and Set 6, 1000 tracks seeks with 20% gain variation.

Simulation results are summarized in the following tables: (subscripts indicate the set number)

	$DOB_1$	$ARC_1$	$DOB_2$	$ARC_2$
$e_M$	.37	.15	.37	.16
$L_2[e]$	.08	.04	.10	.04
$L_2[\Delta u]$	.07	.07	.07	.07
$c_u$	.89	.98	.80	.85

	$DOB_3$	$ARC_3$	$DOB_4$	$ARC_4$
$e_M$	.37	.16	.57	.27
$L_2[e]$	.08	.04	.16	.07
$L_2[\Delta u]$	.12	.19	.12	.15
$c_u$	.63	.63	.53	.58

	$DOB_5$	$ARC_5$	$DOB_6$	$ARC_6$
$e_M$	.56	.39	1.23	.52
$L_2[e]$	.30	.29	.45	.32
$L_2[\Delta u]$	.13	.13	.17	.18
$c_u$	.11	.11	.13	.17

For Set 1 and Set 2, simulation results are also shown in Figure 3.3 and 3.4. The experimental results show that both DOB and ARC except for Set 6 with DOB assure tracking performance with errors smaller than one track throughout the seek transient. Note that

the scales of the upper left plots (for DOB) are twice the scales of the upper right plots (for ARC) in both Figure 3.3 and Figure 3.4. These figures show that ARC is about two times more effective than DOB under the tested conditions. As we can see from the table, in Set 1, the maximum tracking error is 0.37 track with DOB while it is only 0.15 track with ARC. ARC's average tracking performance index  $L_2[e]$  is also two times better than that of DOB despite that ARC is implemented as a discrete time controller. This demonstrates that under external disturbances, ARC is more robust and achieved better performance. When model uncertainties are introduced in Set 2, the ARC approach still does better, with  $e_M$  and  $L_2[e]$  about one half of those of DOB. The advantages of ARC are also shown in Set 3 to Set 6, in terms of both  $e_M$  and  $L_2[e]$ . In simulations, the velocity signal was assumed to be accessible for construction of  $p$  in ARC (see Figure 2.4). In actual hard disk drives, the velocity signal is not directly measurable, and it must be estimated. On the other hand, DOB does not require the velocity signal. In fact, we have thus far successfully implemented only DOB, which will be described in the next Chapter.

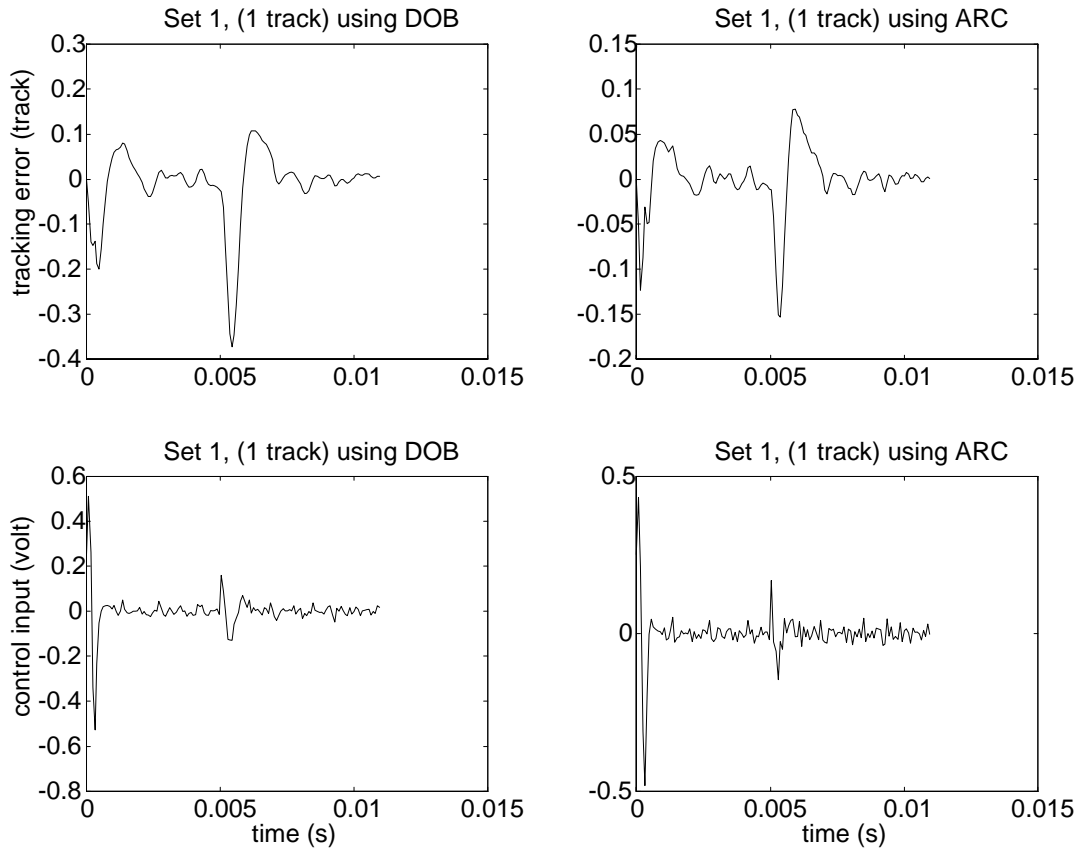


Figure 3.3: Simulation results for Set 1

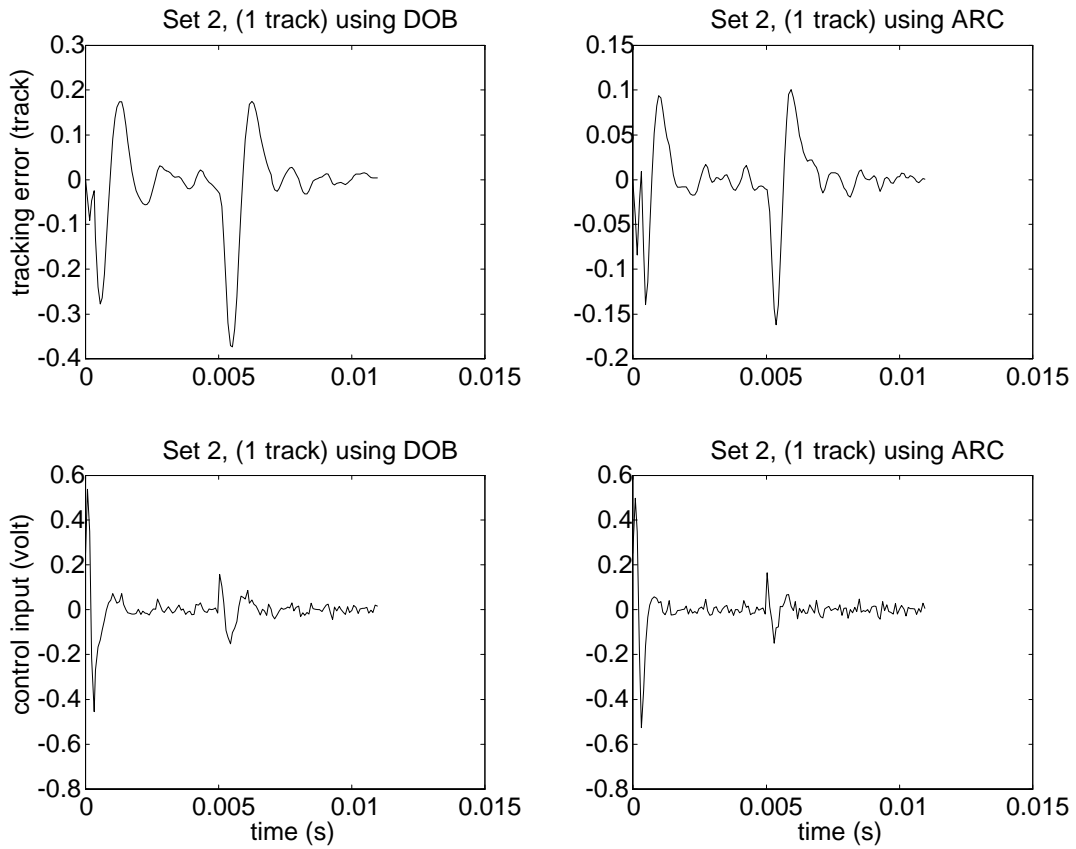


Figure 3.4: Simulation results for Set 2

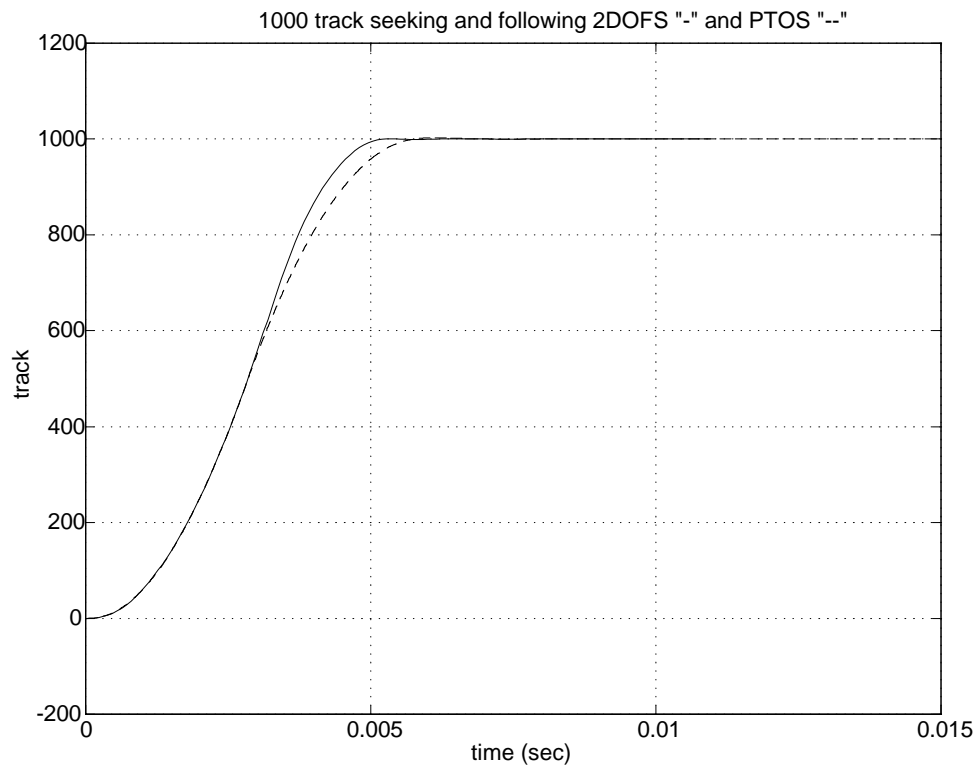


Figure 3.5: 1000 track seeking and following: comparison with PTOS

# Chapter 4

## Fujitsu Drive Track Seeking Experimental Study

### 4.1 Experimental Setup

In this Chapter, advantages of the new reference generation method and robust feedback control are demonstrated by experiments. A Fujitsu 4.3GB SCSI hard disk (model M2954) is used. Model parameters for this drive are:

Spindle speed		7200 <i>rpm</i>
Track pitch	$L_{track}$	3.945 $\mu m$ (6.44kTPI)
Sampling period	$T_s$	67.2 $\mu s$ (14.88kHz)
VCM Coil resistance	$R$	8.516 $\Omega$
VCM Coil inductance	$L$	1.24 <i>mH</i>
Back e.m.f. constant	$K_{eb}$	0.08976 $V \cdot s/rad$
Torque constant	$K_T$	0.08976 $N \cdot m/A$
Moment of Inertia	$I_b$	$5.957 \times 10^{-6} kg \cdot m^2$
1st vibration mode		3.4 <i>kHz</i>

The unit used in experiments is a commercial product, and all servo functions are implemented on a Texas Instrument TMS320C25 fixed-point DSP. For the commercial product, its

DSP leaves little room (memory and computing time) for any modification. Spindle motor controller, state observer, bias compensation, are all in the original assembly code. Because of these hardware and software constraints, it was not possible to test the entire 2DOF controller as proposed in this setup. For instance, It takes approximately 100 machine cycles to implement the proposed reference generator, and another 100 machine cycles to implement DOB or ARC. For TMS320C25 DSP, 100 machine cycles take  $10\mu s$ . It was, however, still possible to implement the proposed reference generation method and the robust feedback control based on DOB separately and confirm their advantages.

## 4.2 Implementation of the New Reference Generation Method

In this experiment, the same feedback controllers are used for the new reference generation method and for the conventional PTOS method. In the reference generator design for this setup, equivalent friction coefficient and spring constant are ignored. Back *e.m.f.*, however, is considered. The comparison results for seeks of 1980 tracks are shown in Figure 4.1. In both upper and lower figures, the first curve is the position signal, the second one is the current signal, and the third one is the seek trigger signal. The seek trigger is low when the hard disk servo is in the seeking mode and high when consecutive 8 samples position signals are within 15% to 20% track near the target track center. The upper figure shows the result of 2DOF system, while the lower one shows that of the conventional PTOS. The proposed new reference generation method achieved faster seeking period (about 1 to 2ms faster). This reference generator can also provide feedforward current information while generating the desired reference trajectory. Such feedforward current can be applied directly to the open loop plant.

However, there are still problems associated with this new method. The switch time for the reference generator has to be at a specific sampling interval. One sample difference of the switch time can cause more than ten tracks difference in the final settling track. In this



case, the 1980<sup>th</sup> track is the settling track for switch time at the 58<sup>th</sup> sample after the seek command was issued. For switch time at the 59<sup>th</sup> sample, the final settling track would be at around the 2007<sup>th</sup> track. Work is in progress to modify the proposed reference generation method for all seeking distances.

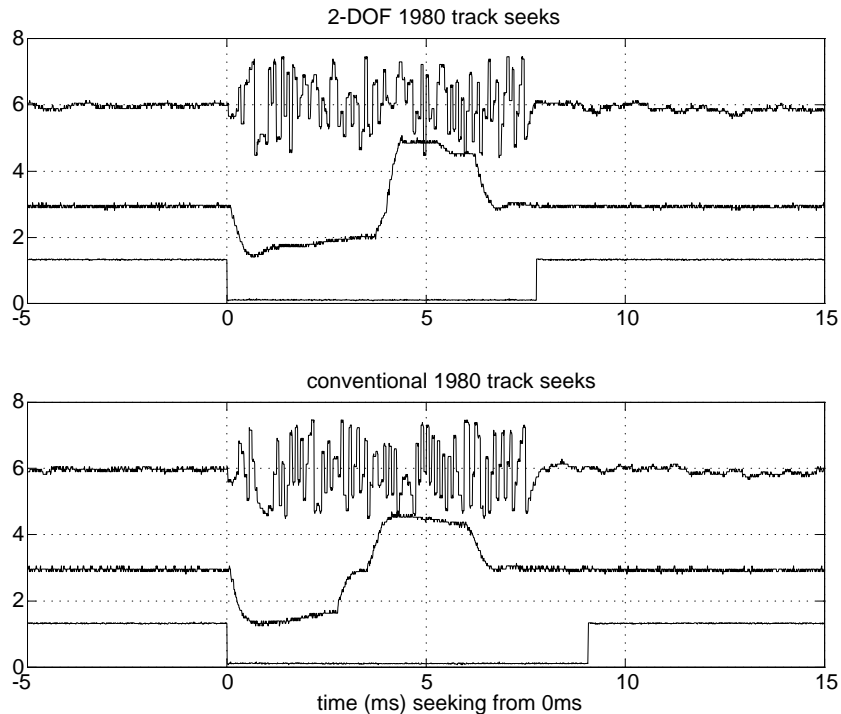


Figure 4.1: Experimental comparison of seeks of 1980 tracks between 2DOF and MSC (Fujitsu hard disk setup)

### 4.3 Implementation of Disturbance Observer

The advantage of robust control can be confirmed for the 2DOF control structure. As mentioned already, it was not possible to implement the robust controller and the proposed reference generator simultaneously. Therefore the reference generator in this experiment

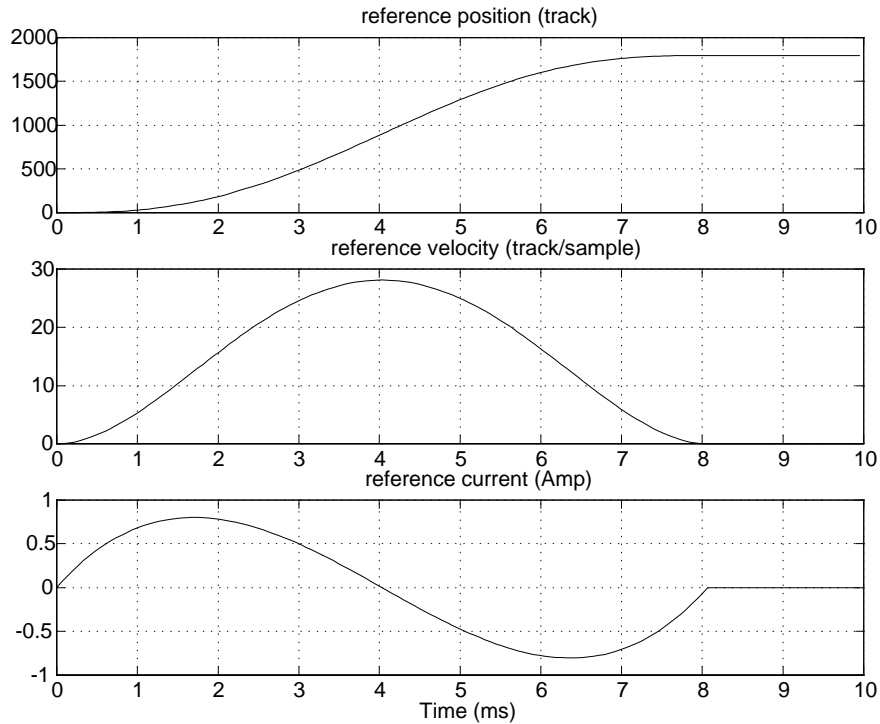


Figure 4.2: SMART reference for seek of 1980 tracks

was computationally less intensive SMART[12], which was a fifth order polynomial profile with three parameters. The SMART reference for 1800 track seek is given in Figure 4.2. Experimental results are shown in Figure 4.3, in which the lower figure is for seek of 1800 tracks for 2DOF with DOB, and the upper one for 2DOFS without DOB. In both figures, the first curve is the position error signal, the second one is the current, and the third one is the seek command trigger signal. For the DOB design, a second order low pass digital IIR filter is used as a  $Q$  filter, whose bandwidth is chosen to be  $350Hz$ . It can be concluded from the experimental results that the use of DOB in the 2DOF control structures decreased the position tracking error during the seek and achieved faster read/write head settling with less seek time.

As seen in Figure 2.4, ARC requires the velocity signal, which is not directly measur-

able. Thus, it must be replaced by its estimate. It was found in the experiments that the performance of ARC is affected by the delay introduced by the state observer. Investigation is in progress to implement ARC in the 2DOF system for HDD control with consideration of such delays.

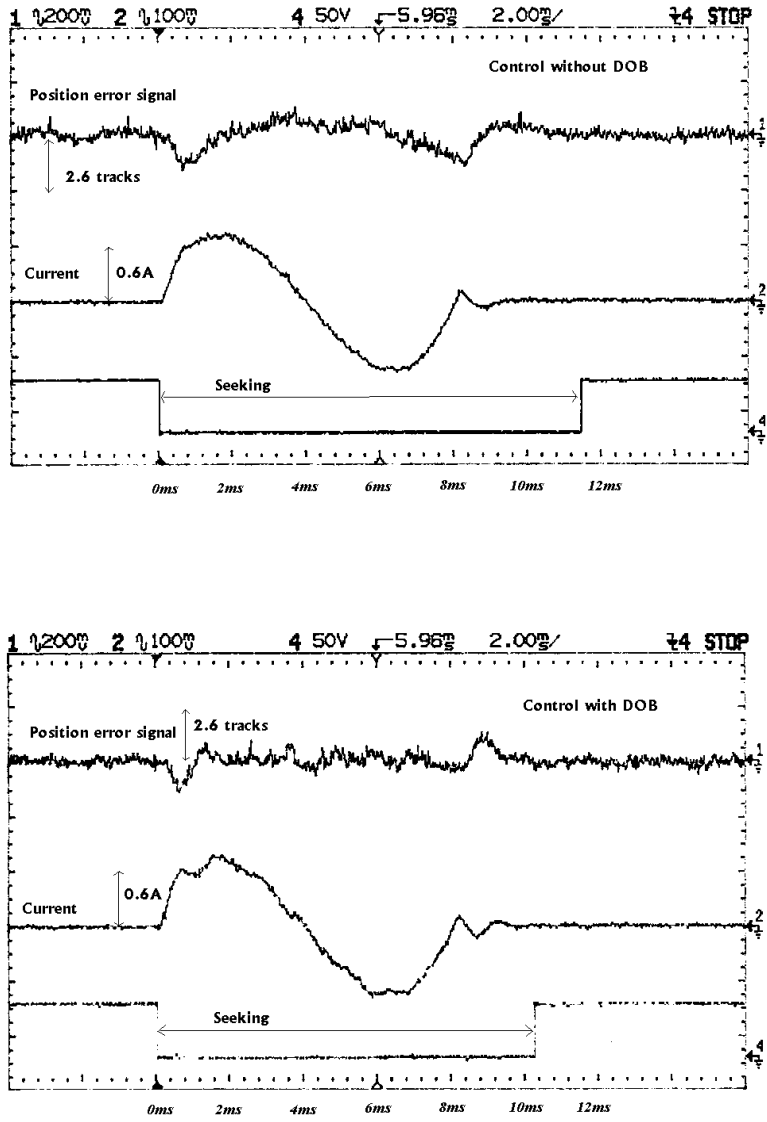


Figure 4.3: Experimental comparisons of 2DOF without DOB and with DOB

# Chapter 5

## High Capacity Drive Track Following Simulation Study

### 5.1 Plant Modeling

To further validate the use of the two-degree-of-freedom servomechanism for disk servo track following control, a simulation study was conducted for a high end drive. Although the drive model uses some fictitious parameters, it still reflects some major characteristics of current high end commercial products in the storage industry. Its high  $20kTPI$  is also among the highest track density of hard drives shipped to the market recently.

The key parameters of the plant model is listed below. The original controller for track following control is a PID type controller. The open loop transfer function of the plant plus the original track following controller is shown in Figure 5.1.

Potential causes of position errors during track following are disk platter noise, sensor and media noise, positional repeatable runout, windage torque, flexible printed circuit (FPC) cable torque, ADC and DAC quantization noise, and electric noise at various places such as the power amplifier and read channels. Those disturbance and noise sources can be categorized into two types based on where they are injected into the servo. Positional disturbances

such as mechanical repetitive runout are injected to the position error signal after the plant; input disturbances such as current noise are injected before the plant. Disturbance and noise model for time domain simulation is shown in Figure 5.5 and 5.7.

Spindle speed		5400 <i>rpm</i>
Track per Inch	<i>TPI</i>	20 <i>kTPI</i>
Sampling period	$T_s$	92.59 $\mu s$
Back e.m.f. constant	$K_{eb}$	0.1 $V \cdot s/rad$
Torque constant	$K_t$	0.1 $N \cdot m/A$
Moment of Inertia	$J$	$5 \times 10^{-6} kg \cdot m^2$
1st Torsion mode		2.5 <i>kHz</i>

## 5.2 Disturbance Observer Design

To evaluate DOB based 2DOF for track following control, DOB is added inside the conventional PID control loop. During track following, the position reference signal given by the reference generator, which in the 2DOF servo structure remains zero. Thus, the reference generator, as well as the feedforward controller, can be ignored.

The discrete DOB introduced in Section 2.4 is used. For  $\tau = 0.001$ , the Q filter has a bandwidth of 351.1*Hz*. The frequency response plots of Q and 1-Q are shown in Figure 5.2.

The closed loop frequency responses from input disturbance to position for system with and without DOB are shown in Figure 5.3. Note that the magnitude is affected by the some scaling factors and only the relative magnitude in the plot is meaningful. The closed loop frequency responses from positional noise to position for system with and without DOB are shown in Figure 5.4. It is observed in Fig. 5.3 that the DOB based controller can strongly attenuates low frequency disturbances up to about 130*Hz*, but it is not effective at frequencies higher than 130*Hz*.

The key point in the DOB design is to understand the noise distribution over all frequencies. The distribution differs depending on products and applications. Trade-offs between attenuation of low frequency noise and some amplification of middle frequency range noise

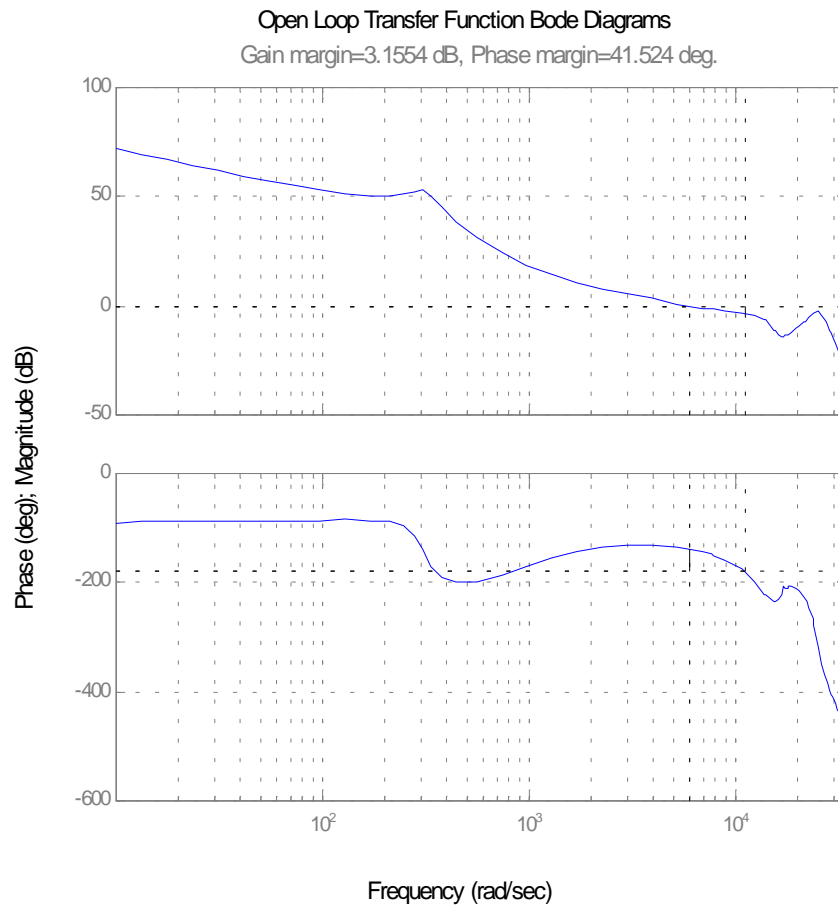


Figure 5.1: Open loop transfer function (plant plus original track following controller)

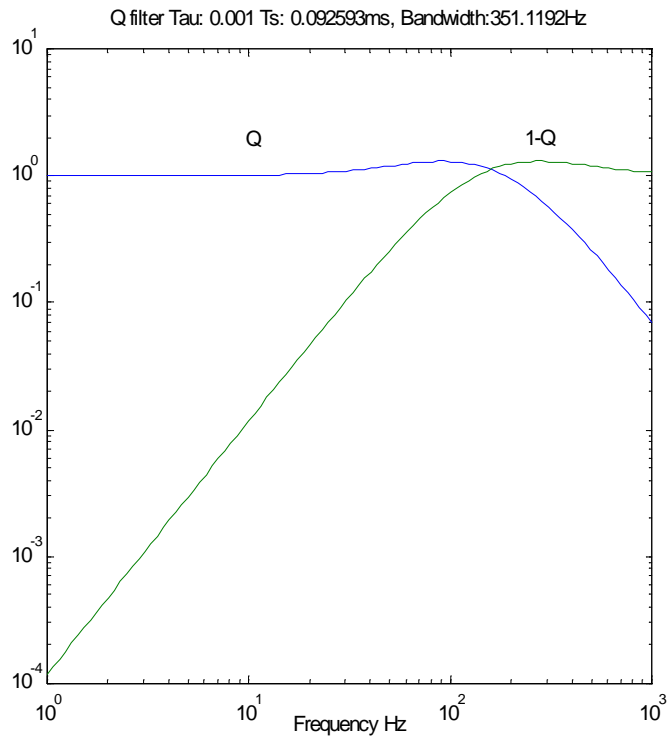


Figure 5.2: Q filter for DOB and 1-Q



depends on the judgement of which part contributes more to the final position error. A criterion is the track misregistration budget, called TMR budget. It is crucial for storage device researchers to understand how much each of the disturbance and noise sources contributes to the position error signal (PES).

For high density disk drives, disturbances at low frequencies contributes more to the TMR budget. Pivot friction is part of the noise source below  $100Hz$ . For portable applications, like hard disks in laptop computers and digital cameras, the external low frequency shock vibration is becoming more serious. In such situations, the use of DOB and other advanced control algorithms have a stronger justification.

### 5.3 Analysis of simulation results

First, assume that there is no radial vibration of the drive. Results of simulations using the original controller for track following is shown in Figures 5.5 and 5.6. Results of simulations using the original controller plus DOB for track following is shown in Figures 5.7 and 5.8. While the improvement gained by DOB may not be very clear in these plots, the statistical analysis performed on the simulation data shows that DOB reduces the variance of PES as much as 15.8%. Results of the statistical analysis are summarized in the following table:

PES summary 0g vibration	$\sigma_1$ w/o DOB	$\sigma_2$ w/ DOB $\tau = 0.001$	Reduction $1 - \frac{\sigma_2^2}{\sigma_1^2}$
<i>PES RRO</i> $3\sigma(\mu\ inch)$	4.50	3.92	24.2%
<i>PES NRRO</i> $3\sigma(\mu\ inch)$	4.45	4.28	7.1%
<i>PES Overall</i> $3\sigma(\mu\ inch)$	6.33	5.81	15.8%

(PES: positional error signal; RRO: repetitive runout; NRRO: non-repetitive runout; variance  $\sigma^2 = E(y(n) - y_m)^2$  where  $y_m$  is the mean of the position error signal time trace  $y(n)$ )

Simulations were repeated by applying a  $60Hz$  radial vibration disturbance, which is equivalent to a sinusoidal acceleration with an amplitude of 0.2g, to the system without

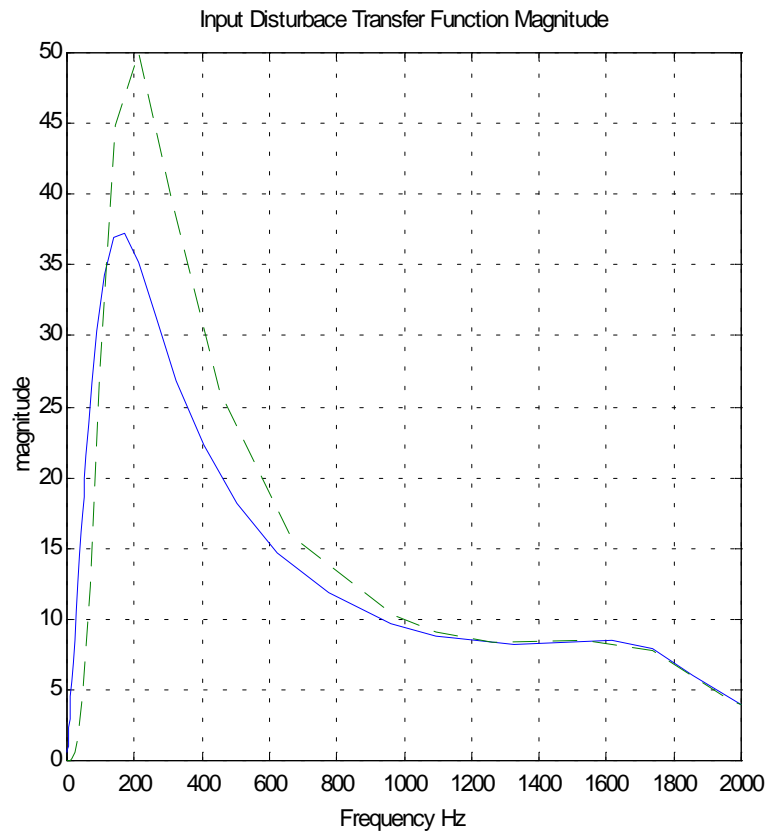


Figure 5.3: Input disturbance transfer function w/o DOB (solid line) and w/ DOB (dashed line).

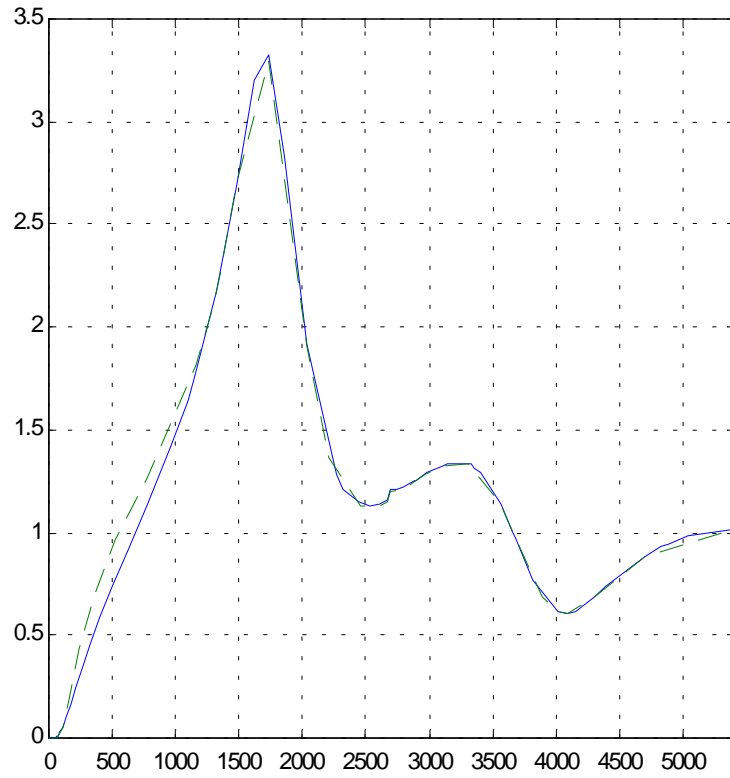


Figure 5.4: Sensitivity Function w/o DOB (dashed line) and w/ DOB (solid line)

DOB and with DOB. Figures 5.9 and 5.10 show the position error signal. In this case, the improvement gained by DOB is evident in these figures.

PES summary	<i>w/o</i> DOB	<i>w/</i> DOB	Reduction
0.2g 60Hz vibration		$\tau = 0.001$	
<i>PES RRO</i> $3\sigma(\mu\text{ inch})$	4.53	3.92	25.3%
<i>PES NRRO</i> $3\sigma(\mu\text{ inch})$	15.89	7.60	77.1%
<i>PES Overall</i> $3\sigma(\mu\text{ inch})$	16.52	8.55	73.2%

The last set of simulations was performed by applying a higher frequency 120Hz radial vibration disturbance, which is equivalent to a sinusoidal acceleration with an amplitude of 0.2g, to the system without DOB and with DOB. Data comparison is as follows:

PES summary	<i>w/o</i> DOB	<i>w/</i> DOB	Reduction
0.2g 120Hz vibration		$\tau = 0.001$	
<i>PES RRO</i> $3\sigma(\mu\text{ inch})$	4.56	4.06	21.0%
<i>PES NRRO</i> $3\sigma(\mu\text{ inch})$	24.6	23.9	5.7%
<i>PES Overall</i> $3\sigma(\mu\text{ inch})$	25.0	24.2	6.2%

In the normal operation condition, PES is reduced by 15%. With 60Hz 0.2g vibration, PES is reduced by 73%. At 120Hz 0.2g vibration, PES is reduced by 6%. These results confirmed the analysis in Section 5.2: at lower frequency, DOB has more attenuation effects on the input disturbance.

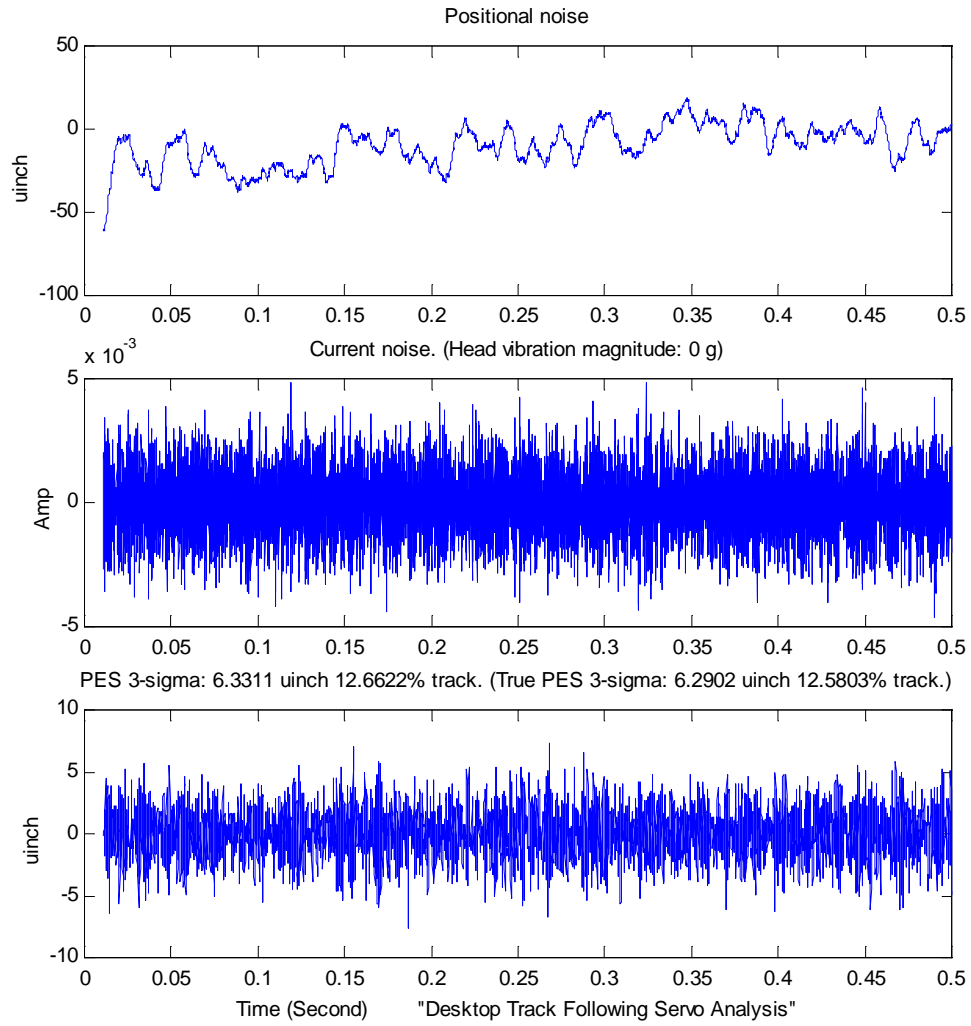


Figure 5.5: Noise disturbance models and simulation results (original track following controller without DOB).

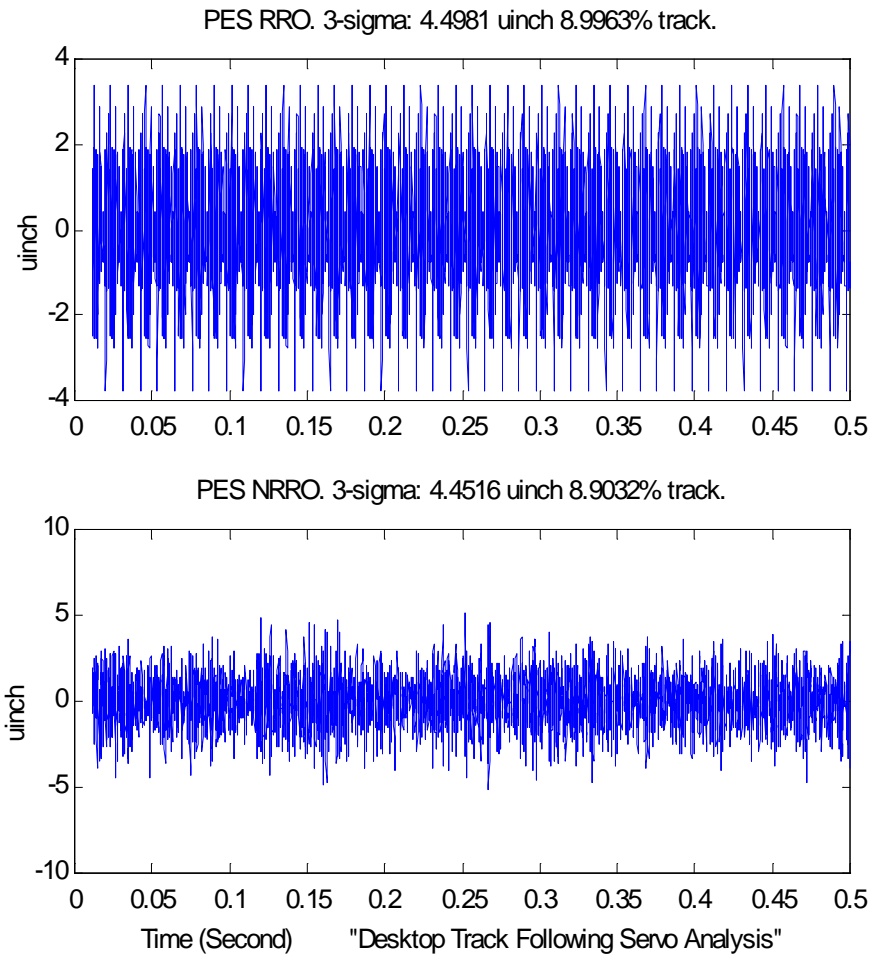


Figure 5.6: RRO and NRRO of PES signal (original controller without DOB) RRO: Repetitive runout; NRRO: non-repetitive runout

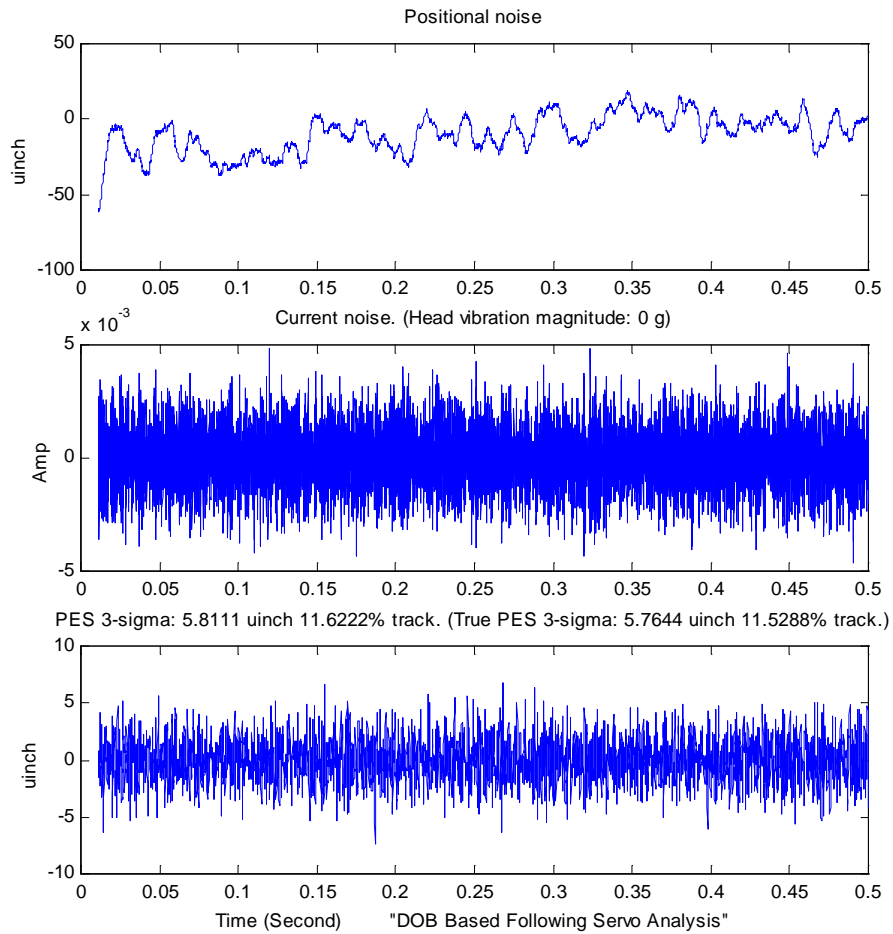


Figure 5.7: Noise disturbance model and simulation results (original track following controller plus DOB).

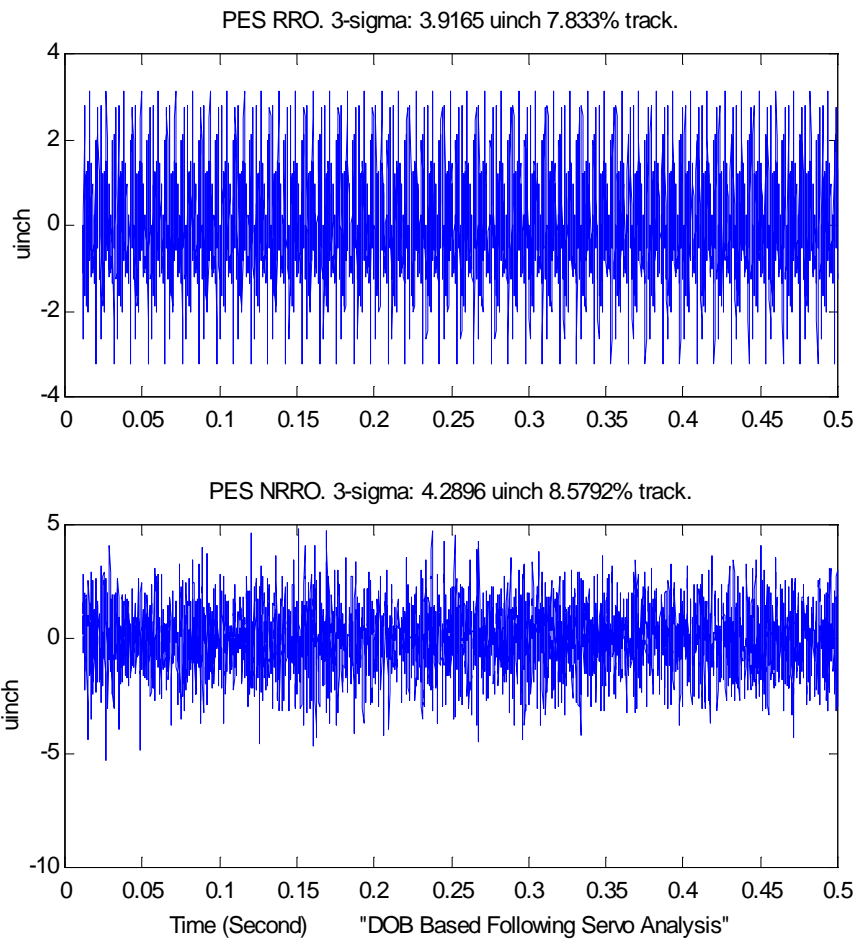


Figure 5.8: RRO and NRRO of PES (original track following controller plus DOB)



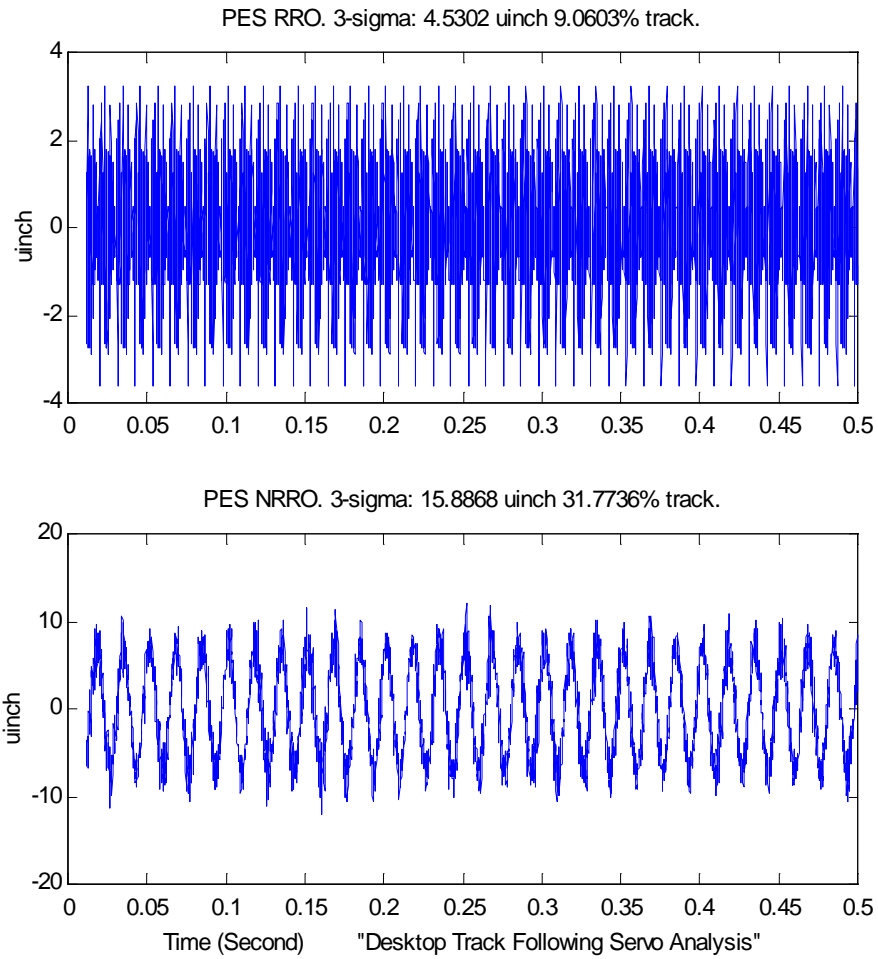


Figure 5.9: NRRO and RRO of PES for 0.2g 60Hz radial vibration disturbance (original track following controller w/o DOB)

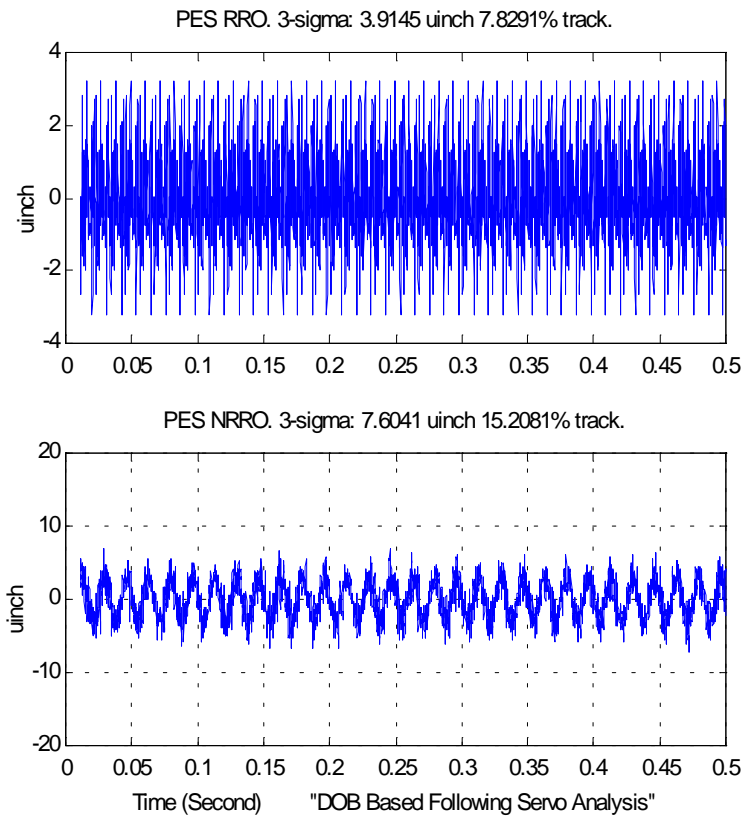


Figure 5.10: NRRO and RRO of PES for 0.2g 60Hz radial vibration disturbance (original track following controller w/ DOB)

# Chapter 6

## Conclusions

This report proposed and investigated a two-degree-of freedom (2DOF) control structure for hard disk drive servo systems. This structure was applied to both track seeking and following control. Two innovative features introduced in this reports are 1) a new method for generating reference signals for track seeking, and 2) two robust feedback control schemes for rejection of disturbances: one scheme uses a disturbance observer (DOB), and the other uses adaptive robust control (ARC).

Simulation results on a  $4.07kTPI$  (track per inch) NEC hard disk drive showed the effectiveness of 2DOF structure with ARC and DOB in both track seeking and tracking control. Comparison are also made between ARC and DOB. Experimental results on a  $6.44kTPI$  Fujitsu hard disk drive setup confirmed the advantage of the new reference generation method and the DOB based 2DOF structure. Simulations results on a  $20kTPI$  hard disk drive also validated the use of DOB for high capacity disk track following control.

## Acknowledgments

This research is funded by the Computer Mechanics Lab in Mechanical Engineering Department at University of California at Berkeley. The authors would also like to thank Professor Bin Yao of Purdue University, Mr. Jun Ishikawa of NEC, Takeyori Hara of Fujitsu Co., Dr. Susumu Hara of JSPS, and Dr. Lin Guo of Maxtor Co. for valuable discussions.

# Bibliography

- [1] J. D. Powell G. F. Franklin and M. L. Workman (2nd Ed.). *Digital Control of Dynamic Systems*. Anderson Wesley, 1990.
- [2] R. Horowitz and Bo Li. Design and implementation of adaptive non-repetitive track-following disk file servos. In *ACC*, pages 4161–4166, Seattle, 1995.
- [3] M. T. White and M. Tomizuka. Increased disturbance rejection in magnetic disk drives by acceleration feedforward control. In *IFAC*, pages 337–342, San Francisco, 1996.
- [4] M. Tomizuka et. al. Disturbance rejection through an external model. *Journal of Dynamics, Measurement, and Control*, 112(6):559–564, 1990.
- [5] H. Lee and M. Tomizuka. Design of friction-compensated and robust digital tracking controllers for high-accuracy positioning systems. In *Japan-USA Symposium on Flexible Automation*, pages 155–162, Kobe, 1994.
- [6] T. Umeno and Y. Hori. Robust speed control of dc servomotors using modern two degrees-of-freedom controller design. *IEEE Transactions on Industry Applications*, 38(5):363–368, 1991.
- [7] M. Tomizuka. On the design of digital tracking controllers. *Transactions of ASME, Journal of Dynamic Systems, Measurement, and Control*, 115:412–418, 1993.

- [8] J. Ishikawa and M. Tomizuka. Pivot friction compensation using an accelerometer and a disturbance observer for hard disk drives. In *ASME International Mechanical Engineering Congress and Exposition*, 1997.
- [9] T. Yamaguchi et. al. Mode switching control design with initial value compensation and its application to head positioning control on magnetic disk drives. *IEEE Transactions on Industrial Electronics*, 43(1):65–73, 1996.
- [10] M.D. Sidman. Time optimal voltage-constrained deceleration velocity profile design for disk drive. In *ACC*, pages 4146–4151, Seattle, 1995.
- [11] B. Yao M. Al-Majed and M. Tomizuka. High-performance robust motion control of machine tools: An adaptive robust control approach and comparative experiments. *IEEE/ASME Transactions on Mechatronics*, 2(2):63–76, 1997.
- [12] Y. Mizoshita S. Hasegawa and K. Takaishi. Vibration minimized access control for hard disk drives. *IEEE Transactions on Magnetics*, 32:1793–1798, 1996.

# Appendix A

## MATLAB function tools

### A.1 Zero Phase Inversion (f\_zp\_inv.m)

see attached program.

### A.2 Decouple Signals into Repetitive and Non-repetitive Portions (fsig2rro.m)

see attached program.

### A.3 Q filter for Disturbance Observer (f\_qfilter.m)

see attached program.

### A.4 ZOH model with Input Delay (f\_zoh\_td.m)

see attached program.

## A.1: f\_zp\_inv.m

```

function [invSS, D] = f_zp_inv (SS)
%F_ZP_INV Zero-phase inversion.
%
% [invSS, D]=F_ZP_INV(SS) returns zero phase inversion (times z^D
% to make causal) invSS of discrete time system SS and sample steps D.
% When invoked without left arguments, F_ZP_INV(SS) plots the bode
% plots of SS*invSS and z^(-D). The phase of the two should overlap and
% magnitude of z^(-D) is unit one and that of SS*invSS should be low
% pass.
%
% Assume SS is strictly stable.
%
%          K*Bc(1/z)*Buc(1/z)
% SS = ----- where Buc(1/z) contains uncancellable zeros,
%          A(1/z)          Buc(1/z) contains cancellable zeros.
%
%          A(1/z)*Buc(z)          Buc(1/z)*Buc(z)
% invSS = ----- so that invSS*SS = -----
%          K*Buc(1)^2*Bc(1/z)          Buc(1)^2
%
% Effects of Bc(z) as a numerator component:
% Buc(1/z) = (z-Zuc) => Buc(z) = (1/z-Zuc) = (1-Zuc*z)/z = -Zuc(z-1/Zuc)/z
% Buc(1)^2 = (1-Zuc)^2
% Introduced zero: 1/Zuc Introduced pole: 0 Introduced gain: -Ze/(1-Zuc)^2
%
% See also SC_DOB.

% error handling
if nargin == 0
    help f_tf2nd
    return
end

% --- get Zeros, Poles, Gain matrix and Sampling time.
[Z P k Ts] = zpkdata(SS);
z = Z{1};
p = P{1};

% --- find Uncancellable zeros index
I_uc = find (abs(z) > 0.99999999);

% --- find Cancellable zeros index
I_c = find (abs(z) <= 0.99999999);

% Initial zeros, poles and gain of invSS
z_inv = p;
p_inv = z(I_c);
k_inv = 1/k;

%
% if ~isempty(I_uc)
%     for idx = 1:length(I_uc)
%         % Effects of Bc(z) as a numerator component:
%         % Buc(1/z) = (z-Zuc) => Buc(z) = (1/z-Zuc) = (1-Zuc*z)/z = -Zuc(z-
%         1/Zuc)/z
%         % Buc(1)^2 = (1-Zuc)^2
%         Zuc = z(I_uc(idx));
%         % Introduced gain: -Ze/(1-Zuc)^2

```



```

        k_inv = k_inv*(-Zuc)/(1-Zuc)^2;
% Introduced zero: 1/Zuc
        z_inv = [z_inv; 1/Zuc];
% Introduced pole: 0
        % But find zeros in z_inv first:
I_z = find(z_inv==0);
if ~isempty(I_z)
    % remove the first zero to cancel the introduced zero pole
    z_inv(I_z(1))=[];
else
    p_inv = [p_inv; 0];
end
end
end

% return zero phase inversion
invSS_true = zpk (z_inv, p_inv, k_inv, Ts);

% steps d
d = length(z_inv) - length(p_inv);

% zero phase inversion with delay D to make it causal
invss = zpk(z_inv, [p_inv; 0*ones(d,1)], k_inv, Ts);

if nargin == 0
    % one sample delay
    d1 = ss(tf(1, [1 0], SS.Ts));
    bode (ss(invss)*SS, d1^d);
else
    D = d;
    invSS = invss;
end

% end of f_zp_inv.m

```

## A.2: fsig2rro.m

```
function [decoupled_sig, sig_matrix] = fsig2rro (sig, n_sectors)
%FSIG2RRO Decouple signals into repetitive and non-repetitive portions
%
% [DS, SM] = FSIG2RRO (SIG, NS) returns decoupled signals DS and
% signal matrix SM. The first column of DS is its repetitive components
% of original signal SIG to be decoupled; the second column is its
% non-repetitive components. (complete revolutions)x(sectors) signal
% matrix SM is the matrix representation of SIG. e.g. sig_matrix (2,14)
% contains signal at the Rev 2, and Sector 14. (All index start from 1)
% NS is the number of sectors per track.
%
% Example:
%   % Load PES data.
%   load ('J:\Transfer\lyi\pes_data\e400nzvd\tlh2id00', 'PE');
%   % Millennium drive spec.
%   S = m_mill;
%   % Decouple NRRO and RRO in micro-inch.
%   fsig2rro(PE/1024/S.TPI*1e6, S.Sector);
%
% See also SPSNOISE.

% Log:
%
% 99-07-01 Li Yi, creation, from Lin Guo's M files.

% error handling
if nargin ~=2
    help fsig2rro
    return
end

% check PES format
if min(size (sig)) ~= 1
    disp ('pes data must be in one column');
    return
end

% data length
length_sig = length (sig);

% Get number of complete revolutions of the PES data
n_revs = floor (length_sig/n_sectors);

%%%%%%%%%%%%%%%%%%%%%%%%%%%%%%%%%%%%%%%%%%%%%%%%%%%%%%%%%%%%%%%%%%%%%%%%
% Save pes to (n_revs)x(n_sectors) matrix (rxs)
%

% loop from 1 to the end of the PES data
for idx=1:length_sig
    % the current rev id (from 1, not 0)
    rev_id = floor (idx/n_sectors) + 1;
    % current sector id (starting from 1 to ns)
    sector_id = rem(idx,n_sectors) + 1;
    % only store the complete revs
    if (rev_id <= n_revs)
        % distribute the signal data to matrix
        rxs(rev_id, sector_id) = sig(idx);
    end
end
end
```

```

% mean of PES at servo sectors
sig_sector_mean = mean (rxs);
% standard deviation of PES at servo sectors
sig_sector_std = std (rxs);

%%%%%%%%%%%%%%%%%%%%%%%%%%%%%%%%%%%%%%%%%%%%%%%%%%%%%%%%%%%%%%%%%%%%%%%%
% re-generate Repetitive and non-Repetitive portion of the signal
for idx=1:length_sig
    % the current rev id (from 1, not 0)
    rev_id = floor (idx/n_sectors) + 1;
    % current sector id (starting from 1 to ns)
    sector_id = rem(idx,n_sectors) + 1;
    % save to temp variable ro
    ro(idx, 1) = sig_sector_mean(sector_id);
    ro(idx, 2) = sig(idx) - sig_sector_mean(sector_id);
end

%%%%%%%%%%%%%%%%%%%%%%%%%%%%%%%%%%%%%%%%%%%%%%%%%%%%%%%%%%%%%%%%%%%%%%%%
% if there is no left argument, plot time trace of pes
if nargin == 0
    clf
    subplot (411)
    plot (rxs');
    grid
    title ('Signals over consecutive periods')
    subplot (412)
    sector_index = 1:1:n_sectors;
    plot (sector_index,sig_sector_mean, '-', ...
        sector_index, sig_sector_mean+sig_sector_std, '--',...
        sector_index, sig_sector_mean-sig_sector_std, '--')
    grid
    title ('Mean and standard deviation of repetitive signals over consecutive
periods')
    subplot (413)
    plot ((rxs-ones(n_revs,1)*mean(rxs))');
    grid
    title ('Non-Repetitive signals over consecutive periods')

    subplot (414)
    plot (sector_index, mean(rxs-ones(n_revs,1)*mean(rxs)), '-', ...
        sector_index, mean(rxs-ones(n_revs,1)*mean(rxs))+std(rxs-
ones(n_revs,1)*mean(rxs)), '--',...
        sector_index, mean(rxs-ones(n_revs,1)*mean(rxs))-std(rxs-
ones(n_revs,1)*mean(rxs)), '--');
    grid
    title ('Mean and standard deviation of non-repetitive signals over
consecutive periods')
    xlabel ('Servo Sectors')
else
    sig_matrix = rxs;
    decoupled_sig = ro;
end

% end of file fsig2rro

```

### A.3: f\_qfilter.m

```
function [SS, BW] = f_Qfilter (TAU, Ts)
%F_QFILTER Q filter for Disturbance Observer.
%
% [SS, BW] = F_QFILTER (TAU, TS) returns discrete Q filter for Disturbance
% Observer and its bandwidth BW. If Ts is omitted, then it returns the
% continuous time domain Q filter. When invoked without left argument,
% F_QFILTER plots bode plots of the Q and 1-Q.
%
% Continuous time domain Q filter:
% 
$$Q(s) = \frac{3 \cdot \text{TAU} \cdot s + 1}{(\text{TAU} \cdot s)^3 + 3 \cdot \text{TAU}^2 \cdot s^2 + 3 \cdot \text{TAU} \cdot s + 1}$$

%
% See also SC_DOB.

% error handling
if nargin < 1
    help f_qfilter
    return
end

% Continuous time domain Q filter
Q = tf([3*TAU 1], [TAU^3 3*TAU^2 3*TAU 1]);

% Frequency points Hz
f = logspace (0, 3, 100);
% Frequency points Radian
w = 2*pi*f;

% Obtain magnitude response mQ
if exist('Ts')
    % Discrete time Q filter
    Q = c2d (Q, Ts, 'tustin');
    [mQ pQ wQ] = dbode (Q.num, Q.den, Ts, w);
else
    % Continuous time domain Q filter Bandwidth
    mQ = bode (Q, w);
end

% Process mQ to obtain Bandwidth
I = find (mQ <= 0.5);
if ~isempty(I)
    f_bw = f(I(1));
    bw = num2str(f_bw);
else
    bw = '>3K';
end

Qi = 1 - Q;

if nargin >= 1
    % Return outputs
    SS = Q;
    BW = bw;
else
    % Plot Bode
    if exist ('Ts')
        [mQi pQi wQi] = dbode (Qi.num, Qi.den, Ts, w);
        loglog (f, mQ, f, mQi)
```

```
        title (['Q filter Tau: ' num2str(TAU) ' Ts: ' num2str(Ts*1e3) ...
              'ms, Bandwidth:' bw 'Hz']);
    else
        bode (Q, 1-Q);
        title (['Q filter Tau: ' num2str(TAU) ' Bandwidth:' bw 'Hz']);
    end
end
% end of f_qfilter.m
```

## A.4: f\_zoh\_td.m

```
function SS_Td = f_zoh_Td (SS, Ts, Td)
%F_ZOH_TD Discrete time system with input delay.
%
%   SS_TD = F_ZOH_TD (SS, TD) returns the discrete time domain
%   SS data SS_TD of the zero order hold (ZOH) model of continous
%   time system SS using sampling time Ts and with a ZOH delay of
%   Td.
%
%   See Page 49 of <<Computer-Controlled Systems>> 2nd edition,
%   by Karl J. Astrom. For linear discrete time with ZOH delay:
%
%    $x(k+1) = Ax(k) + B0*u(k) + B1*u(k-1)$ 
%    $B0 = \int_{0 \rightarrow Ts-Td} \{ \exp(As)*ds*B \}$ 
%    $B1 = \exp(A(Ts-Td))*\int_{0 \rightarrow Td} \{ \exp(As)*ds*B \}$ 
%
%   See also M_LIGHT

% error handling
if nargin ~= 3
    help f_zoh_td
    return
end

% Get the A, B, C, D of continous time system SS
[A B C D] = ssdata (ss(SS));

% Zoh model for sampling time Ts-Td
[A0 B0 C0 D0] = c2dm(A, B, C, D, Ts-Td, 'zoh');

% Zoh model for sampling time Td
[A1 B1 C1 D1] = c2dm(A, B, C, D, Td, 'zoh');

% Zoh model for sampling time Td
SS_D = c2d (ss(SS), Ts, 'zoh');
[A_D B_D C_D D_D] = ssdata(SS_D);

B1 = expm(A*(Ts-Td))*B1;

ss_td = ss([A_D B1; zeros(1, length(A_D)) 0], [B0; 1], [C_D 0], D_D, Ts);

if nargout == 0
    bode (ss_td, ss(SS));
else
    SS_Td = ss_td;
end

% end of f_zoh_td
```